UNIVERSITÀ POLITECNICA DELLE MARCHE

DIPARTIMENTO SCIENZE DELLA VITA E DELL'AMBIENTE

Corso di Laurea Magistrale

BIOLOGIA MOLECOLARE E APPLICATA

Produzione ricombinante, caratterizzazione mediante diffusione a piccolo angolo dei raggi X e saggi funzionali della proteina beta-amiloide

Recombinant production, characterization by small-angle X-ray scattering, and functional assays of the beta-amyloid protein

Tesi di Laurea Magistrale
di:

Sofia Ventura

Relatore
Chiar.mo prof.

Francesco Spinozzi

Correlatore:

Lucia Silvestrini

Sessione Estiva
Anno Accademico 2021/2022

TABLE OF CONTENTS

ABSTRACT…..……4

1 INTRODUCTION ……7

1.1 History of fibrils ……..…8

1.2 The processing of APP and the genesis of Aβ peptides..……9

1.3 The β-amyloid peptides……...12

1.4 Amyloid fibrils……..….15

1.5 The kinetics of aggregation…….21

2 AIM OF THE THESIS……..27

3 MATERIAL AND METHODS ……30

3.1 Plasmid ……31

3.2 competent cells…… ……32

3.3 culture media……32

3.4 Buffers……...…33

3.5 Antibiotics…….……34

3.6 Methods ……34

3.6.1 Plasmid recovery……...36

3.6.2 Transformation……36

3.6.3 Protein expression……38

3.6.4 Cell lysis……39

3.6.5 Protein purification……40

3.6.6 Analysis of the purified protein……40

3.6.6.1. SDS-Page and protein sequencing……40

3.6.6.2. Spectrophotometric determination of the protein concentration..41

3.6.6.3. Small-angle X-Ray Scattering……41

3.6.6.4. Functional assays with Thioflavin T in fluorescence spectrometry……49

4 RESULTS……52

4.1 Production and purification of Aβ ……53

4.2 Aβ analysis……53

4.2.1 SDS-Page ……53

4.2.2 Sequencing……56

4.2.3 Small-angle X-Ray Scattering……57

4.3 Thioflavin T assay……60

5 CONCLUSION…….……..….64

6 BIBLIOGRAPHY……..….67

ABSTRACT

La presenza di placche di amiloide-beta (Aβ) è un segno distintivo della malattia di Alzheimer. Capire come questa proteina inizialmente solubile si ripiega e contribuisce alla degenerazione, è fondamentale per lo studio della malattia. Molti studi sull'aggregazione e la tossicità dell'Aβ attualmente utilizzano l'Aβ ottenuto per sintesi chimica grazie alla facilità di acquisto e alla poca manipolazione richiesta per ottenere l'Aβ allo stato monomerico; tuttavia, le differenze nei protocolli di disaggregazione possono anche introdurre strutture eterogenee nel peptide di partenza. L'HFIP è ampiamente utilizzato per disaggregare l'Aβ, ma può anche portare alla formazione di strutture oligomeriche, poiché il peptide viene portato a pH neutro tramite il suo punto isoelettrico e alla formazione di strutture aggregate.

Su queste basi, la presente tesi mira a produrre la proteina Aβ42 ricombinante da E. Coli, aggirando alcune delle questioni sopra sollevate. La mia tesi si è concentrata sulla produzione della proteina beta-amiloide, in modo semplice e relativamente veloce. Vari fattori hanno contribuito alla produzione di questa proteina, il fatto che il promotore del plasmide fosse un promotore molto forte (T7), ha permesso, sotto induzione, una produzione della proteina in grande quantità nei corpi di inclusione di Coli BL21. La produzione nei corpi di inclusione, in questo caso, è stata un fattore di aiuto, in quanto la proteina rimane isolata da tutte le altre componenti cellulari e può essere purificata

semplicemente rompendo i corpi di inclusione. Uno dei fattori chiave nello studio della proteina beta amiloide (soprattutto 42) è averla in forma monomerica, che con questo protocollo si ottiene, anche se per un tempo limitato. Grazie alla sua produzione, è stato possibile eseguire studi SAXS preliminari delle prime strutture proteiche aggregate. Inoltre, in seguito ai dati di sequenziamento e ai saggi in Tioflavina T, è stato possibile sia valutare la correttezza della proteina prodotta sia misurarne la risposta al colorante fluorescente. In particolare, la concentrazione ottimale di 25 μM di ThT e Aβ riflette il rapporto 1:1 raccomandato in questo tipo di saggio.

Grazie alla possibilità di ottenere un Aβ ricombinante, sarà possibile in futuro studiarne a fondo la struttura ei molteplici stati conformazionali che esso forma in relazione alle condizioni fisico-chimiche, comprendere come Aβ assembla in fibrille, e, soprattutto, quali strategie possono essere applicate per studiarne l'inibizione.

Chapter One

INTRODUCTION

1.1 History of fibrils

In 1854, the German physicist Rudolph Virchow directed his studies on macroscopic anomalies in the human brain (described for the first time in the liver in 1639, lardaceous liver), present in the form of corpuscles, in concentric layers, and resembling grains of starch, the amylacea corpora. These corpuscles, like starch, reacted positively to iodine staining, tinged with blue while all other tissues were colored yellow. Instead, treatments with iodine and sulfuric acid, used as tests for cellulose in the cell membrane of plants (Unger, Goldmann, 1847), revealed the characteristic violet color of the cellulose. Hypothesizing "cellulose-like" substances, Virchow coined the term "amyloid" (Cohen, 1986). Subsequent studies (Friedreich and Kekulè, 1859) instead demonstrated the presence, in these amyloid masses, of protein material, a significant quantity of nitrogen, and, above all, the absence of carbohydrates, for which it was thought that the "amyloid" was a protein or class of proteins that formed structurally amorphous clusters. Microscopy studies with polarized light have shown that the accumulations of amyloid in a large number of tissues, not stained and colored with Congo-red, exhibited a positive birefringence to the longitudinal axis of the deposits. [1] Congo-red staining imparted marked anisotropy to the "apple green" birefringence of amyloid fibrils in situ. Therefore, birefringence after Congo Red staining was the first

criterion adopted to define amyloid. In 1959, Cohen and Calkins, through electron microscopy studies, showed that amyloid deposits of different origins all exhibited a comparable fibrillar ultrastructure in fixed sections of tissue: bundles of rigid and linear fibrils, ranging in width from 60 to 130 Å and in length between 1000 and 16000 Å. The fibrillar morphology was, therefore, the second criterion by which amyloid was defined. Finally, X-ray diffraction analysis of isolated amyloid fibrils [2] revealed that they were ordered in a secondary structure called Cross-β. In this structure, the skeleton of the polypeptide assumes the β − sheet conformation, and, while the β-strands are oriented perpendicular to the fibrillar axis, the face of the β sheet (antiparallel) is parallel to the fibrillar axis. This is the last criterion that is used to define amyloid.

1.2 The processing of APP and the genesis of Aβ peptides

The amyloid precursor protein, or APP, is a type I integral membrane glycoprotein, having a large N-terminal glycosylated domain on the extracellular side and a smaller intracellular C-terminal domain. It is encoded by the APP gene, on the long arm 17 of chromosome 21, and abundantly expressed in a wide variety of tissues [3]; There are several isoforms of APP but the predominant form in the human brain is APP695, produced mainly by neurons [4]. The role of this protein is not yet fully understood but it seems

important in regulating neuron survival, neurite development, synaptic plasticity, and cell adhesion. Since, after synthesis, a large fraction of APP molecules is transported along the axon up to the presynaptic terminal, one of its possible functions is that of a surface receptor, which initiates the transduction pathway of the intracellular signal following the binding with an extracellular ligand [5]. (Fig.1)

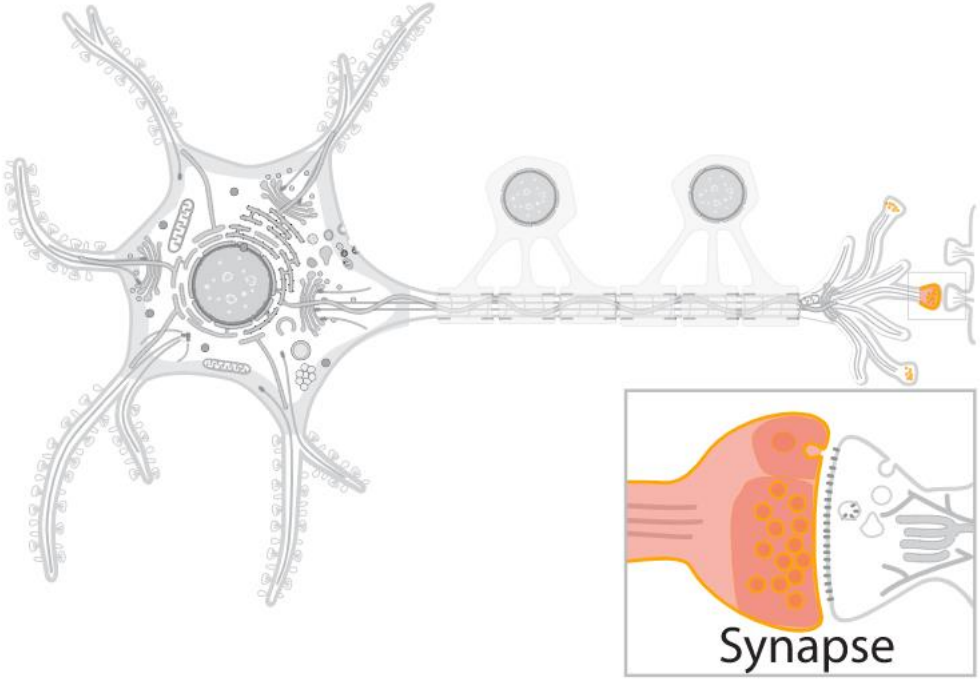

Figure 1: Pre-synaptic localization of APP. [6]

Furthermore, the expression of APP is up-regulated during the maturation and differentiation of neurons [7]. APP is subject, under physiological conditions, to two processing pathways, one non-amyloidogenic (α-secretase pathway) and one amyloidogenic (β-secretase pathway), which leads to the production of and

one amyloidogenic (β-secretase pathway), which leads to the production of Aβ peptides. (fig.2) [8].

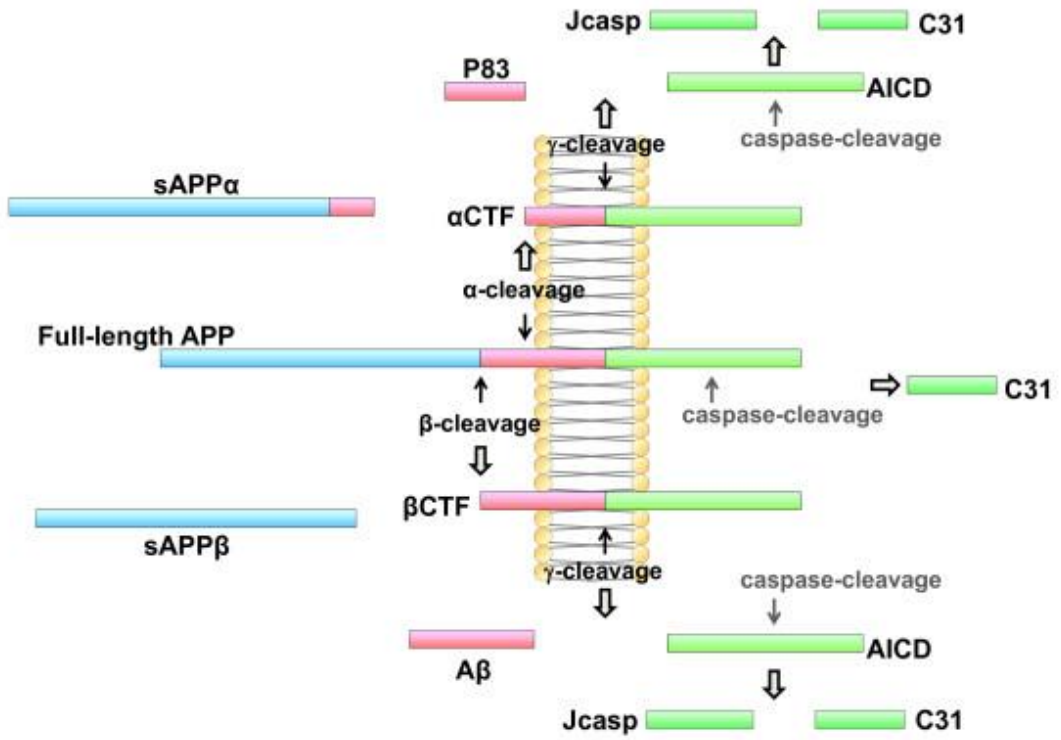

Figure 2:Schematic diagram of APP processing (not drawn in proportion). It is not clear whether caspases cleave membrane-associated APP forms or released AICD. [9]

Firstly, the cut of the α-secretase on the extracellular side generates the soluble fragment sAPPα, which is secreted, and the fragment C83, which remains anchored to the membrane and is subject to the subsequent action of the γ-secretase, with the formation of the p3 fragment, released from the membrane. This pathway is non-amyloidogenic since α-secretase cuts within the sequence of the Aβ peptide. In the amyloidogenic pathway, however, the proteolytic

cleavage by β-secretase on the extracellular side occurs at the level of the extreme N-terminal of the Aβ sequence, with the formation of the sAPPβ fragment, secreted and C99, which remains in the membrane. [fig.2]

The latter is then attacked by γ-secretase, which cuts in different positions at the C-terminal end of the Aβ sequence. The result is the formation of β-amyloid fragments between 39 and 43 amino acids in length, of which the most abundant are Aβ40 and Aβ42, which are secreted, and an "intracellular domain of APP" (AICD, APP Intracellular Domain), which it plays a role in the regulation of calcium-mediated signals and, once translocated to the nucleus, functions as a transcription factor [10; 11; 12].

In healthy and young individuals, Aβ peptides are completely catabolized shortly after being secreted by cells, before they can accumulate while, with advancing age, the intensified production and their reduced clearance can determine their deposition and subsequent aggregation, with neuronal degeneration [13]. Most Alzheimer's cases are sporadic, not hereditary; however, there appear to be many genes that determine some susceptibility to the disease. The first of these is the gene for apolipoprotein E, for which three alleles encode the 19 isoforms E2, E3, and E4; E4-producing individuals are at high risk of disease, since this isoform appears, on the one hand, to intensify the amyloidogenic pathway of APP processing and, on the other hand, to favor

the aggregation of Aβ peptides and reduce their clearance [14]. This promotes cerebrovascular disease, increased oxidative stress, and loss of synaptic plasticity. Cases of familial (hereditary) Alzheimer's represent 5-10% of total cases and are mainly due to the change of one or two amino acids, within the Aβ sequence or adjacent to it, which favor the amyloidogenic pathway of proteolytic cleavage, and/or to mutations in the genes of PreSenilin 1 (PS1) and PreSenilin 2 (PS2), which alter the activity of γ-secretase [15].

1.3 The β-amyloid peptides

As mentioned above, from the proteolytic double cut catalyzed by β- and γ-secretase, Aβ peptides of variable length are generated but the main constituents of the amyloid plaques are the Aβ (1-40) and Aβ (1-42) peptides [16]. Except for the two C-terminal amino acids, Ile41 and Ala42, the sequence of the two peptides is identical. Despite the high degree of homology, Aβ40 and Aβ42 show profoundly different behavior both in vivo and in vitro. The concentration of secreted Aβ42 is about 10% of that of Aβ40, yet Aβ42 is the main component of the plaques, and its neurotoxicity is found to be much higher [17]. Furthermore, the aggregation process of Aβ42 is significantly faster in vitro than that of Aβ40 and the two peptides follow very different fibrillogenesis pathways. The behavior of the two peptides seems to diverge in the early stage of assembly, probably due to the presence of the two

"additional" amino acids; in fact, Aβ40 is present, in vivo, in the form of monomers, dimers, trimers and tetramers in equilibrium with each other, while Aβ42 is initially present in the form of unstructured monomers which tend to oligomerize early in pentamers and hexamers, which are also mainly not structured, called paranuclei. It seems that the critical residue for their formation is Ile41, whose side chain would also promote the self-assembly of paranuclei into larger oligomers [18,19,20]. (Fig.3)

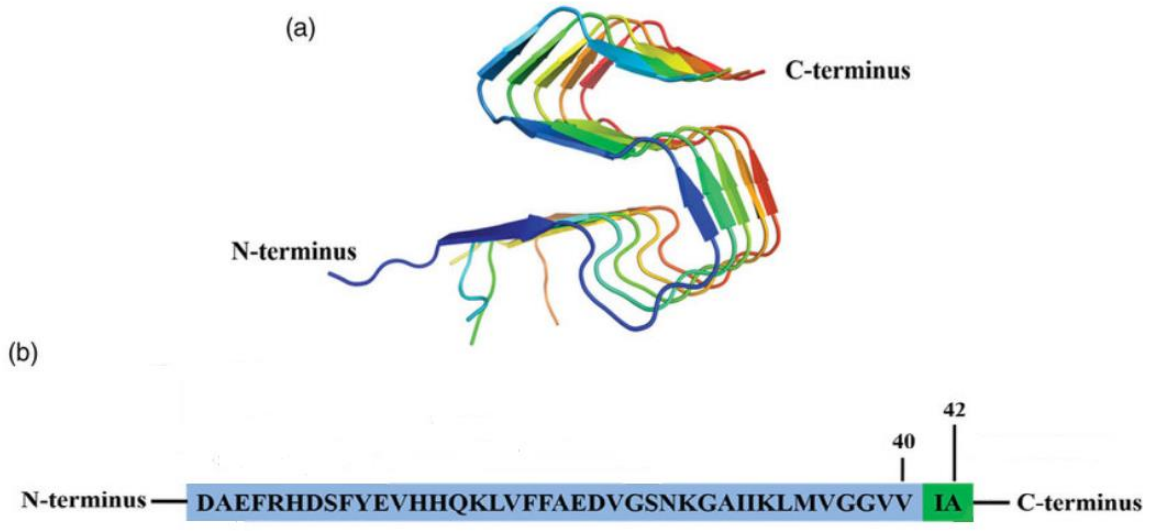

Figure 3: Figure 3: Structure and sequence of the amyloid-b protein (Ab). (a) A typical 3D structure of Ab fibrils. (b) Amino acid sequence of Ab and different recombinant variants [21].

Despite the neurotoxicity resulting from their accumulation, Aβ peptides, under physiological conditions, seem to have a potential role linked to the maintenance of synaptic plasticity and neuronal survival. Since the APP protein is transported along the axon to the presynaptic terminal and processed there,

the synapses are the sites where the Aβ oligomer can accumulate in high quantities; being Aβ secreted in the presynaptic space, the effects deriving from its possible accumulation are expressed on the integrity and functionality of both the pre-and postsynaptic terminals, which therefore represent the sites from which the possible death of the neuron begins, for both necrosis and apoptosis [22].

If the cellular machinery responsible for the disposal of Aβ is not efficient, there is inhibition of long-term potentiation (a form of memory-related synaptic plasticity) and memory loss even in the absence of amyloid deposits or evident neuronal degeneration [23;24]. The mechanisms of neuronal degeneration promoted by the Aβ peptide appear to be mainly related to oxidative stress of membrane proteins, DNA, and lipids. Aβ-induced lipid peroxidation reduces the functionality of many ionic ATPases, glutamate, and glucose transporters, and GTP-binding proteins [25]. As a consequence, there is a perturbation of ionic homeostasis and the main cellular solutes; in particular, it seems that Aβ significantly alters calcium homeostasis through oxidative stresses that disable the calcium pumps on the membrane and favor the flow of this ion through voltage-dependent channels or ionotropic receptors for glutamate; more recent studies also suggest that this peptide directly promotes calcium flux, itself forming non-specific channels in the membrane or activating surface receptors

coupled to calcium passage [26]. An increased concentration of intracellular calcium can induce hyperactivation of calcium-dependent proteases or kinases and, the latter, can cause hyperphosphorylation, and therefore aggregation, of tau proteins [27]. To confirm this hypothesis, it has been observed that neurons containing neurofibrillary tangles show a high amount of Ca2 + inside them. The inability of neurons to regulate calcium ion homeostasis, whose role is fundamental for learning and memory processes, is an aspect of Alzheimer's pathogenesis that appears to be intimately related to synaptic dysfunction and neuronal death [28].

1.4 Amyloid fibrils

The accumulation of proteins in the form of amyloid fibrils is common in a large number of neurodegenerative disorders. Although the proteins involved in these diseases are not related to each other either in structure or function, the insoluble amyloid aggregates possess surprisingly similar characteristics. All show fibrillar morphology, predominant secondary structure β-sheet, insolubility in common solvents and detergents, high resistance to proteases, green birefringence after Congo red staining, and ability to bind to Tioflavine T [29]. Amyloid fibrils are semi-flexible structures, typically linear and about 6-12 nm wide; they are formed by a variable number, from 3 to 6 usually, of extended filaments (protofilaments) of about 1-2 nm in diameter, rolled up to

form a "rope" structure [30] .The growth of each protofilament proceeds in a bidirectional way, by apposition of new oligomeric units while the lateral association of several protofilaments gives rise to the large amyloid fibrils. (Fig.4)

As mentioned before, the ordered "core" of the amyloid fibrils is represented by a cross-β structure, where each protofilament consists of a double row of β-

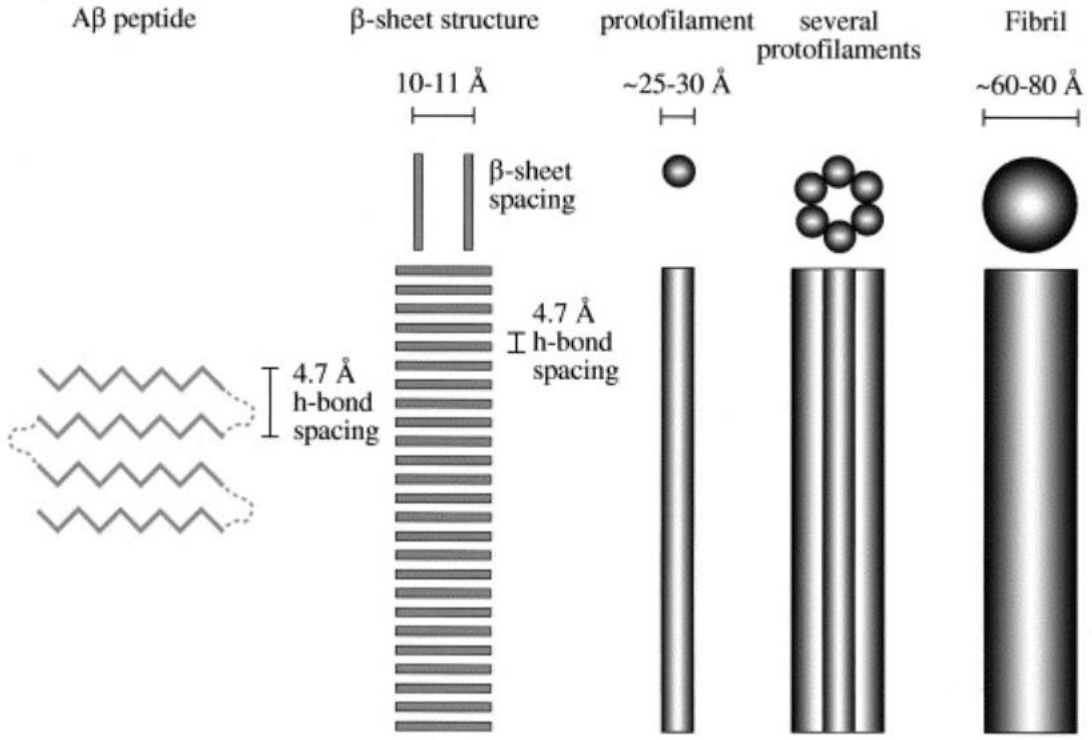

Figure 4:This figure shows the hierarchy of structure from the Aβ peptide folded into a β-pleated sheet structure through protofilaments to amyloid fibrils. Views shown looking down the axis of the fibre and axially. [31]

sheet; this is the secondary structure in which each monomer is organized,

whose β-strands run parallel to each other and perpendicular to the main axis of the fibril [32]. (Fig.5)

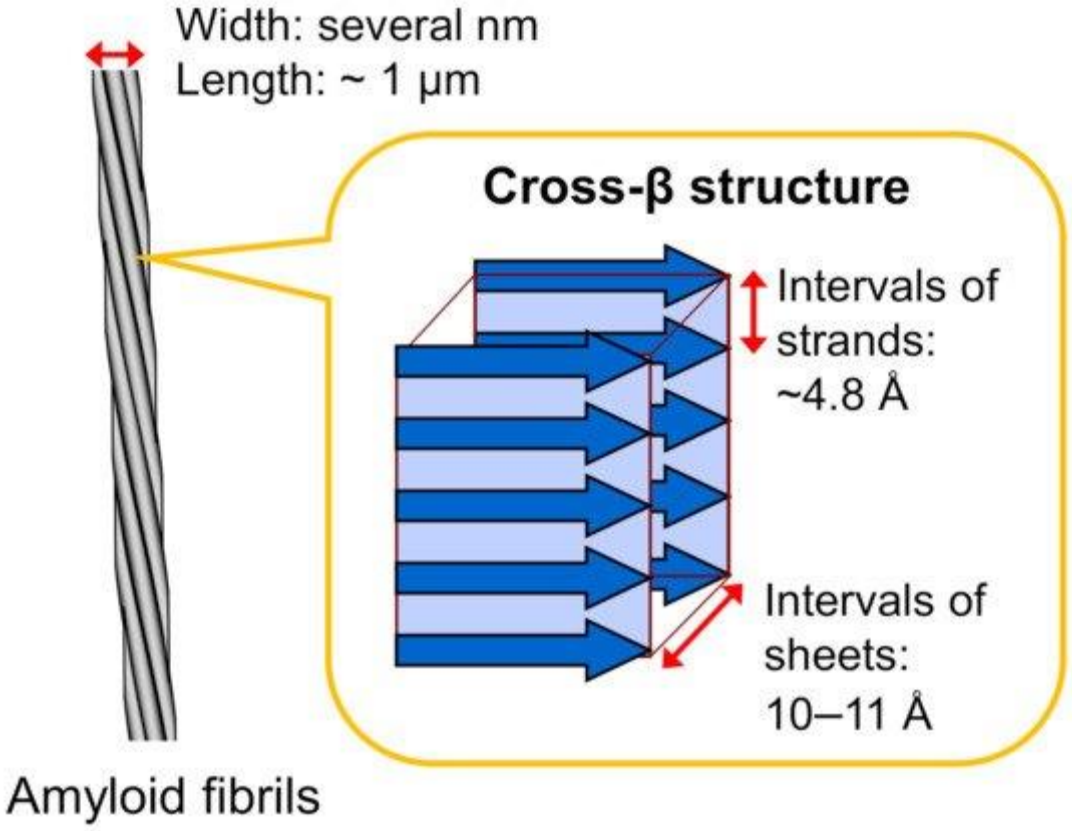

Figure 5:Schematic illustration of the structure of an amyloid fibril. Amyloid fibrils typically show needle-like and unbranched morphology, which consists of several protofilaments a few nanometers in width and around a micrometer in length that are laterally.[33]

The cross-β structure of the "core" is the characteristic invariant structure of amyloid fibrils and it has been hypothesized to be an energetic minimum for all aggregated proteins [32] as well as the probable cause of their optical properties [33] further the architecture of the amyloid core. The β-strands are joined by H-bridges in an antiparallel rearrangement in the direction of the fibril, forming long β-sheet "ribbons", which, in turn, are parallel and in register and are

arranged staggered in the direction of the main chain. The βsheets are held together by interactions, especially electrostatic, between the side chains of the amino acids. The N-terminal of the β-strand associates with the C-terminal of another β-strand, allowing the aromatic side chains to interact. A compelling feature of the similarity between amyloid peptides is the high occurrence of aromatic residues, which stabilize the packing of the layers through π-π stacking interactions. In particular, the Phe-19 residue of the β-amyloid protein appears to be particularly important in the formation of fibrils. If Phe-19 is replaced with another amino acid, for example, Ala, the ability to form fibrils is completely lost [34]. The most common techniques for identifying fibrils are based on the use of two dyes: Congo Red and Thioflavin T. Although both are known as histological dyes, they have also proved useful for in vitro studies of isolated amyloid deposits and fibrils in solution. In the presence of fibrils, both undergo specific changes in their spectroscopic characteristics.

Congo Red-stained amyloid fibrils exhibit intense apple-green birefringence in polarized light; however, the mechanism of interaction between the two molecules remains unclear. Although it has been the first technique used to detect the presence of fibrils, its exclusive use can result in false negatives; in fact, it has recently been observed that Congo Red can bind not only insoluble

fibrils but also soluble oligomers and that the amyloid core does not show birefringence after staining [35].

Thioflavin T (Th T) is a benzothiazole dye that exhibits intense fluorescence when bound to amyloid fibrils and is the most commonly used technique for diagnosing the presence of fibrils both ex vivo and in vitro. The structure of Th T, shows below, has a hydrophobic terminal with a dimethylamine group attached to a phenolic group, in turn, linked to a benzothiazole group, more polar because it contains N and S. (Fig. 6).

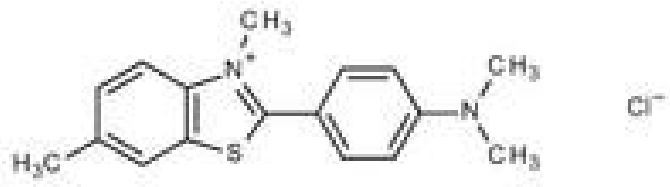

Figure 6:Molecular structure of the fluorescent probe Thioflavine T [36] .

This combination of polar and hydrophobic regions gives the molecules of ThT the possibility of forming micelles in an aqueous solution, with the hydrophobic interior and the positively charged N facing the solvent. This may indicate that the thiazole nitrogen of the pigment and a hydroxyl group in the samples form H bonds that give rise to the specific bond between the Th T and the amyloid fibrils . In an aqueous solution Th T, if excited at λ = 342 nm, shows a fluorescence peak at 430 nm; exciting at longer wavelengths, λ = 442nm or λ

= 450 nm, the pigment has a very low fluorescence emission but, in the presence of fibrils, the emission spectrum shifts towards red and has an intense peak at 482 nm [37]. A possible cause of the low quantum fluorescence efficiency of Th T in an aqueous solution seems to be the breakdown of the conjugated bonds, due to the mutual reorientation of the benzothiazole and benzoamine rings. If the molecule is not excited, its configuration is rather planar but, following excitation, there is a transfer of charges between the aromatic rings, which leads to a non-equilibrium state, in which the charges are separated. This state can be stabilized if the π-conjugated bond system is broken and one of the rings rotates 90 ° toward the other; in this situation, the charges cannot return to their original distribution, and this explains how the fluorescence emission has such a low efficiency. Following the binding with the amyloid fibrils, mainly due to charge interactions, a steric restriction of the rotation of the two rings of the Th T occurs, due to the rigidity of the microenvironment, and this seems to be the cause of the high quantum fluorescence efficiency [38]. Another possible cause is that the positive charges of the Th T micelles, exposed to the solvent, can form specific H bonds with the amyloid fibrils, inducing changes in the excitation spectrum which are reflected in an increase in fluorescence emission.

1.5 The kinetics of aggregation

The fibrillogenesis of Aβ is a polymerization process whose time course is represented by a sigmoid curve, characteristic of all nucleation-dependent aggregation kinetics [39]. The kinetics of this type of process are characterized by two key parameters: the nucleation rate and the elongation rate of the fibrillar aggregates [40]. The initial self-assembly is slow and proceeds until the aggregates reach a critical size; once the “nucleus” is formed, the growth of the aggregates by apposition of new monomers proceeds rapidly .In the initial phase (lag phase or nucleation phase) no aggregation is observed but the entropically disadvantaged process of association of free monomers begins, which proceeds up to the formation of nucleation seeds , which are oligomers of variables size that favor the aggregation process.

These "seeds" provide a sort of "template" capable of recruiting further monomers, thus increasing the size of the growing aggregates [41]. From this point on, the kinetics proceeds rapidly (log phase or phase of polymerization), until the formation of metastable aggregates with fibrillar morphology

(protofibrils). The last phase of the aggregation kinetics (plateau) is characterized by the formation of mature, very stable fibrils. (Fig.7).

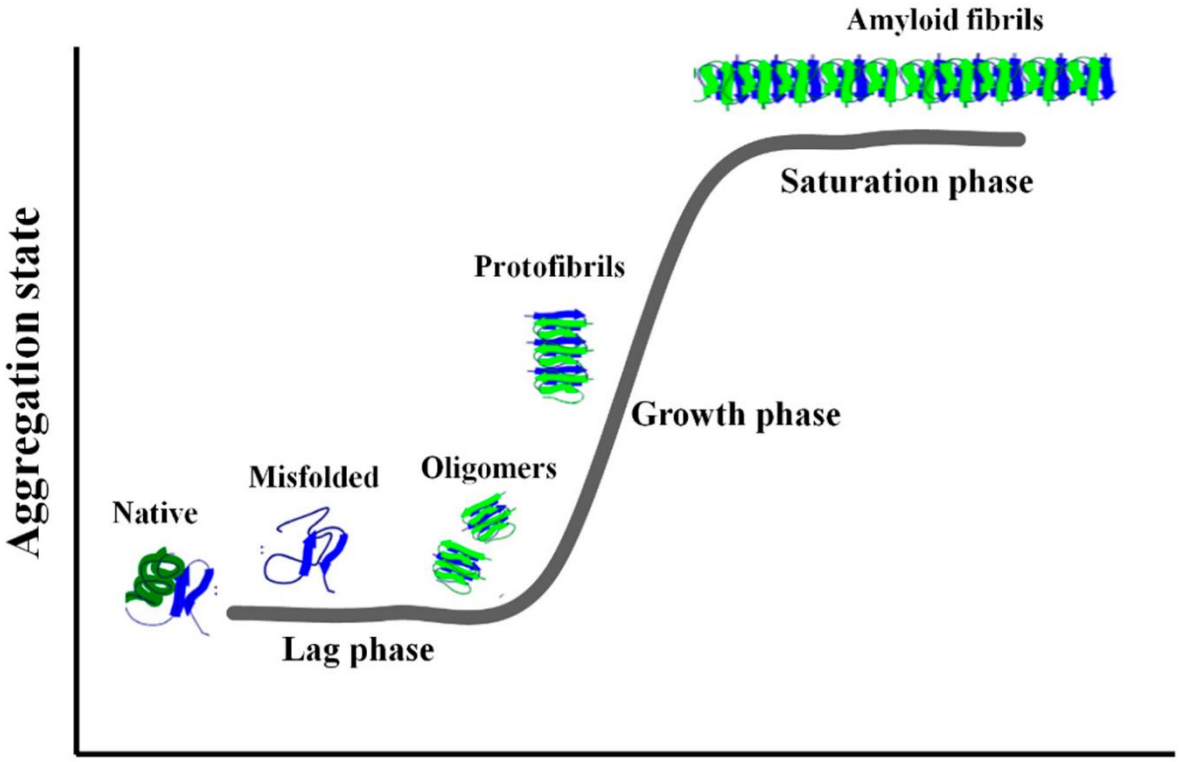

Figure 7: Nucleation-dependent fibril formation process The sequence of events along the fibril formation pathway includes: (Lag phase) aggregation of misfolded monomers into small intermediate oligomers; (Growth phase) re-arrangement of these oligomers into an organized conformation containing the cross beta structure (Saturation phase) association of beta structured oligomers into proto-fibrils and finally into fibrils[42].

The aggregation kinetics of the fibrillogenic process has a sigmoidal trend typical of nucleation-dependent polymerizations characterized by a latency phase, a polymerization phase, and a saturation. The presence of pre-existing impurities or aggregates can modify the trend of the curve, giving rise to kinetics that cannot be reproduced from an experimental point of view, in which the latency phase could be considerably reduced or even absent. The lag phase does not depend on the time required for nucleation, but on the time required

for the growth of sufficiently large aggregates [42]. About the polymerization of Aβ, this phase represents the critical point of the entire process since any presence of pre-aggregates can cause a drastic reduction in duration or even disappearance. Immunological and radiochemical tests have confirmed the hypothesis that polymerization is a process in which Aβ oligomerizes, through a series of short-lived intermediates, that form protofibrils, which act as templates for the growth of mature fibrils. Indeed, oligomers of intermediate size between monomers and protofibrils have been observed but none of them accumulate in significant quantities. Initially, the monomers associate to form dimers that accumulates during fibrillogenesis; then, the time-dependent decrease in the number of dimers is parallel to an increase in the number of protofibrils [43]. Protofibrils are relatively stable intermediates, originating from nuclei, and are the first particles of fibrillar morphology that can be detected [44]. They have been found about 200 nm long and 4-10 nm in diameter, are flexible and slightly curved, and are visible only transiently during Aβ fibrillogenesis, confirming the hypothesis that they may be the real precursors of mature, longer, and more rigid fibrils [45].

Several mechanisms have been proposed to explain the transition from protofibrils to fibrils. The simplest involves the "end-to-end" association of protofibrils but this is rather unlikely since, being a substantially controlled

diffusion process, it is very difficult for the protofibrillar ends to meet and align correctly. The protofibrils could, on the other hand, associate laterally to form "auto templates", to which the precursors (monomers and dimers) can bind and polymerize, or the lateral association could accelerate the "end-to-end" association [46]. Mature fibrils, analyzed under the electron microscope, appear more rigid than protofibrils but of rather heterogeneous morphology. They are long, linear, consisting of five or six "protofilaments" ,wrapped to form β helices and have 32 repetitions every 115 Å or 250 Å, which reflect the winding of the protofilaments. Longer fibrils, in which coiling and alignment have probably reached the highest degree, appear in two different forms: thinner "type I" fibrils, and larger and larger "type II" fibrils late in earance.[46] Circular dichroism measurements indicate that protofibrils have a content of β structures (β-sheet and β-turn,)> 50%, random coil 40%, and α-helix 10% practically equivalent to that of mature fibrils. (Fig.8).

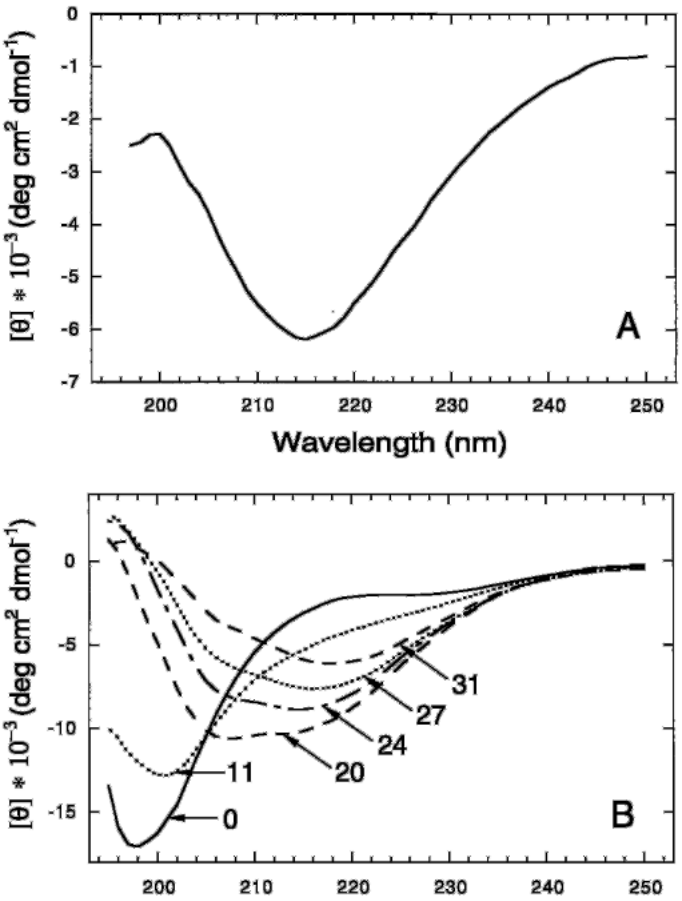

Figure 8: Secondary structure analysis of protofibrils and LMW Ab. CD spectroscopy was performed on freshly isolated protofibrils (A)and LMW Ab.(B) Protofibrils and LMW Ab concentrations were 18.5 and 54 mM, respectively. In the case of LMW Ab, spectra were taken immediately upon isolation, then after 11, 20, 24, 27, and 31 days. Results are expressed as molar ellipticity [Q] (deg cm2 dmol21). The data shown are representative of those obtained in each of five independent experiments..[47]

The modest α-helix content in the protofibrils makes it possible that, during the fibrillogenesis of low molecular weight peptides (LMW-Aβ, Low molecular weight-Aβ), a conformational change occurs from a predominantly random coil initial structure to a final rich in β-sheet, passing through transient α-helix intermediates.[48]

Chapter Two

AIM OF THE THESIS

The presence of beta-amyloid (Aβ) plaques is a hallmark of Alzheimer's disease. Hence many research efforts have been dedicated to understand how this initially soluble protein folds and contributes to the disease. Many studies on Aβ aggregation and toxicity currently makes use of Aβ obtained by chemical synthesis due to the ease of purchase and little manipulation required to obtain Aβ in the monomeric state. However, commercially available synthetic Aβ is quite expensive, should be reconstituted to remove oligomers, a process that can lead to the loss of proteins in the form of insoluble structures, and there is often variation in the resulting samples due to the use of different solvents for the reconstitution, which can affect the structure of the monomers. Differences in disaggregation protocols can also introduce heterogeneous structures in the starting peptide, such as the use of hexafluoroisopropanol (HFIP).

HFIP is widely used to disaggregated Aβ, but it can also lead to the formation of oligomeric structures, as the peptide is brought to neutral pH via its isoelectric point. Synthetic Aβ has been reported to have high batch variability and lower toxicity than recombinantly produced Aβ. In Aβ production, tagged purification is a very popular method as it improves solubility, allows the use of affinity capture chromatography, and provide highly pure recombinant Aβ samples. However, if the tags are not removed before further analysis of the peptide, even a small tag, such as a 6xHis tag, can greatly affect protein

structure and propensity for aggregation. Furthermore, the removal of the tag requires the addition of a cleavage recognition site and further purification steps, which may lead to protein loss, increased protein handling time, and ultimately the formation of aggregated species. [49]

The protocol of Walsh et al. [50] provides a simple method for purification of AβM variants by using urea solubilization to isolate AβM from inclusion bodies, purification by ion exchange chromatography and size exclusion chromatography, centrifugation by applying a 30 kDa filter, and lyophilization for storing the recombinant protein. However, the DEAE-cellulose chromatography medium used in the ion exchange step is not easy to find and use. As with all intrinsically disordered amyloidogenic proteins, the structure of the starting material, the presence of multimers or degraded products, and the surrounding environment heavily influence the rate of aggregation, the aggregation pathways that are undertaken, and the toxicity of the resulting amyloid. On these bases, the present thesis aims to produce the recombinant Aβ42 protein from E. Coli, bypassing some of the outlined issues raised above.

Third chapter

MATERIALS AND METHODS

3.1 Plasmid

The plasmids were purchased from the Addgene company. For the production of the Abeta protein was used: Pet-Sac-Abeta (M1-42) and Pet-Sac-Abeta (M1-40). (fig.9;fig.10)

Pet-Sac-Abeta (M1-42).

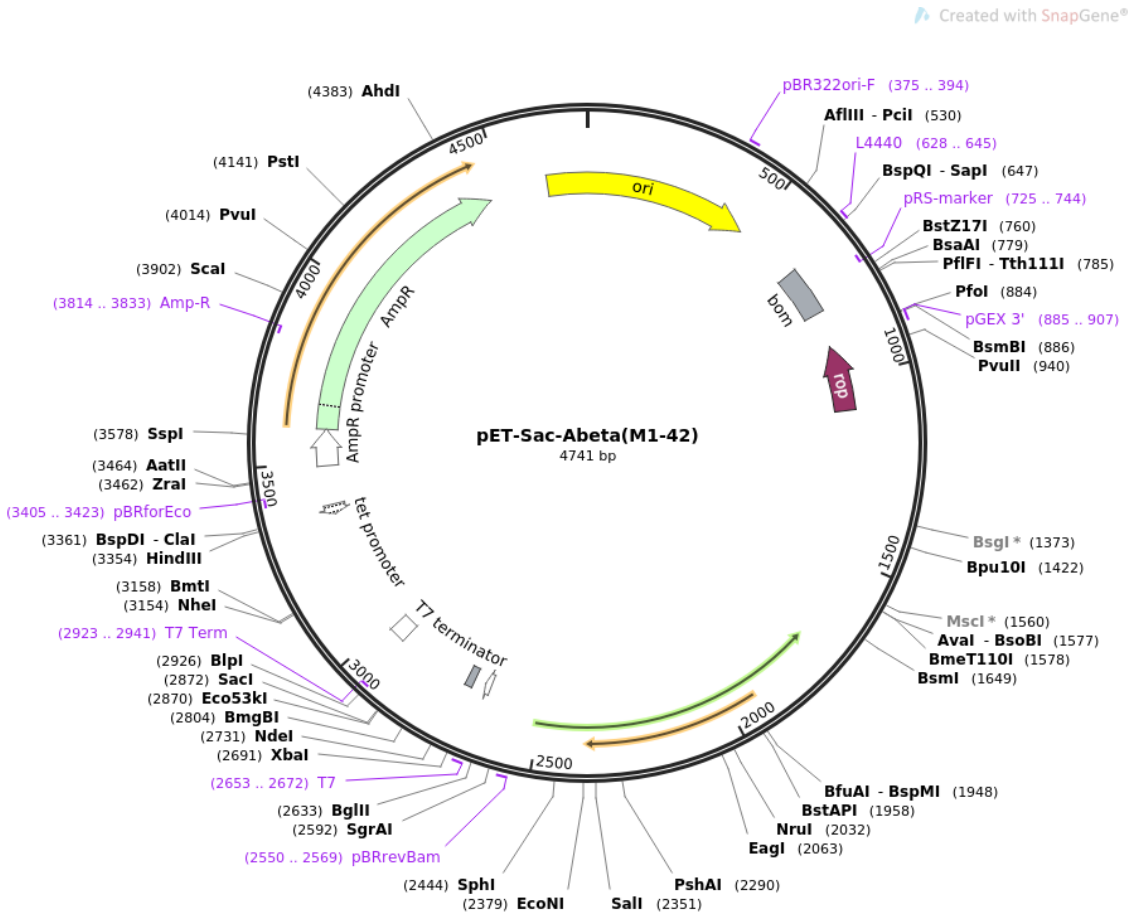

Figure 9: Abeta 42

Pet-Sac-Abeta (M1-40)

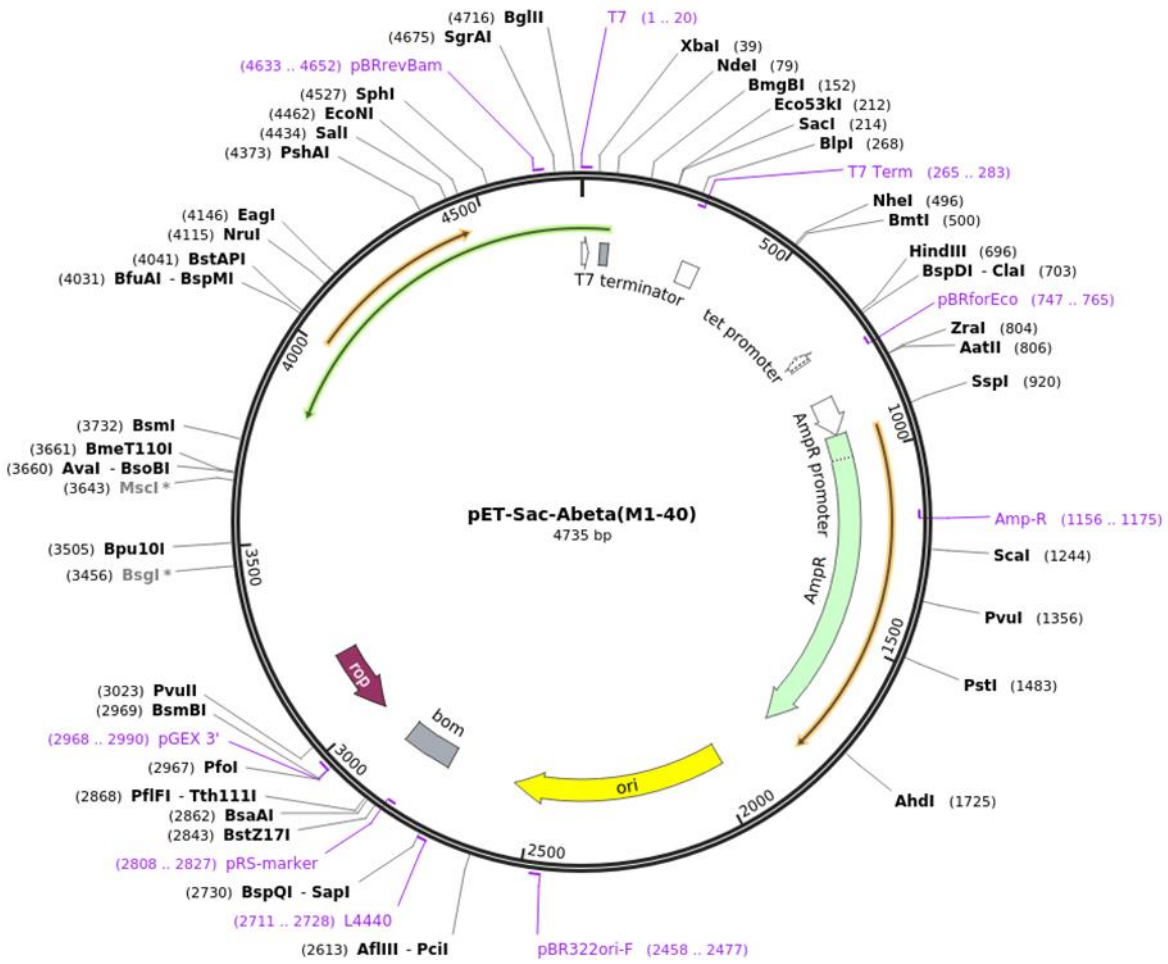

Figure 10: Abeta 40

3.2 Competent cells

For the expression of the target protein in bacteria, E. coli BL21 derived cells from the Termo-Fisher company were used: Oneshot BL21 (DE3) pLysS Chemically Competent E.Coli.

3.3 Culture media

The medium LB (Luria Bertani) was used in both liquid and solid form.

For a Liter: 1% Tryptone

0.5% yeast extract

1% g NaCl

The solution must be brought to volume with deionized water and stirred to dissolve the powders, then the medium must be sterilized by autoclave. To make the LB medium in solid form (plates), 15 g /L of Agar should be added to the LB in the liquid form already described. This medium should also be autoclaved and allowed to cool so that it can allow for the possible addition of antibiotics, which otherwise would be degraded by a temperature above 50°C. The liquid should be poured into sterile plates and left to solidify. Both of these operations must be carried out under the biological hood.

3.4 Buffers

The buffers used for the cell lysis phase are:

10 mM Tris 1 mM EDTA pH 8	
Buffer A	Buffer B
	8 M Urea

The main solution must be brought to volume with deionized water and the pH must be corrected to 8 thanks to the use of HCl.

The buffer used for the electrophoretic run-in agarose is the TAE.

For a 50X liter: 242 g Tris Base

57.1 mL Glacial Acetic Acid

100 mL EDTA 0.5M pH 8

The solution should be brought to volume with deionized water and stirred to dissolve the powders. Being 50X TAE, it is diluted for use in running as 1X TAE.

The buffer used for the acrylamide electrophoretic run is TGS.

For a 10X liter: 0.25 M tris Base

1.92 M glycine

1% SDS

The solution should be brought to volume with deionized water and stirred to dissolve the powders. Being 10X TGS, it is diluted using it in the race as 1X TGS.

3.5 Antibiotics

Antibiotics		
Abbreviation	Full name	Concentration
Amp	Ampicillin	100 mg/mL
Clo	Cloramphenicol	34 mg/mL

3.6 Methods

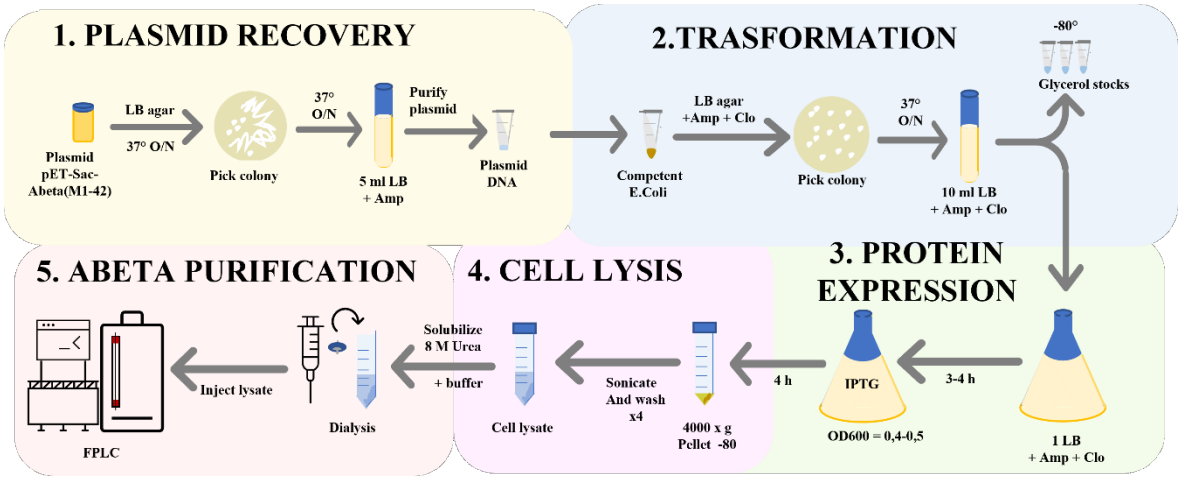

Figure 11: Production protocol

3.6.1 Plasmid recovery

The plasmid is delivered in an agar bacterial culture. A small percentage of plasmid was removed using a sterile loop from the corresponding bottle and sown on LB agar plates with the antibiotic Ampicillin at the concentration described above. The plate was grown at 37°C overnight, the following day a single colony was taken using a sterile loop to start a bacterial mini culture in 5 mL of LB and Amp, to obtain a higher number of cells from which to extract the plasmid. The growth was carried out overnight at 37°C with an agitation of 220 rpm. The following day the plasmid extraction was performed with the kit: Plasmid Plus Midi kit(Qiagen). As a control, an agarose gel electrophoresis was performed. The agarose gel was prepared at a percentage of 1%. The samples were prepared by combining the plasmid in solution with the loading dye and deionized water, then the run was performed in 1X TAE buffer for approximately 30 minutes at 80-100 V. The bands were visualized by UV using

a gel imaging system. The plasmid concentration at 260 nm absorbance was measured with a spectrophotometer. Typical plasmid yield is 40-45 ng/µL in 5 mL of LB culture.

The extracted plasmid was frozen at -20°C.

3.6.2 Transformation

Both the extracted plasmid and the competent cells were thawed on ice. For the expression of Pet-Sac-Abeta (M1-40) in bacteria, cells of the Escherichia Coli BL21 strain subjected to thermal shock were used. Once thawed, 2 µL of plasmid was added to the competent cells (to give approximately 50 ng of total DNA). The cells and the plasmid were incubated on ice for 20 min and then placed in a bath thermostated at 45°C for approximately 45 s. After the thermal shock, the vial was kept on ice for another 2 min. To the transformed bacteria were inoculated 800 µL of LB without any antibiotic and kept in a thermostat at 37°C for one hour. Subsequently, about 25 µL of the 500 µL were plated in LB plates containing the antibiotics Ampicillin and Chloramphenicol at the concentrations indicated. About five minutes were waited under a fume hood to allow the cells to absorb onto the LB agar. Then was grown at 37°C overnight. (fig.12).

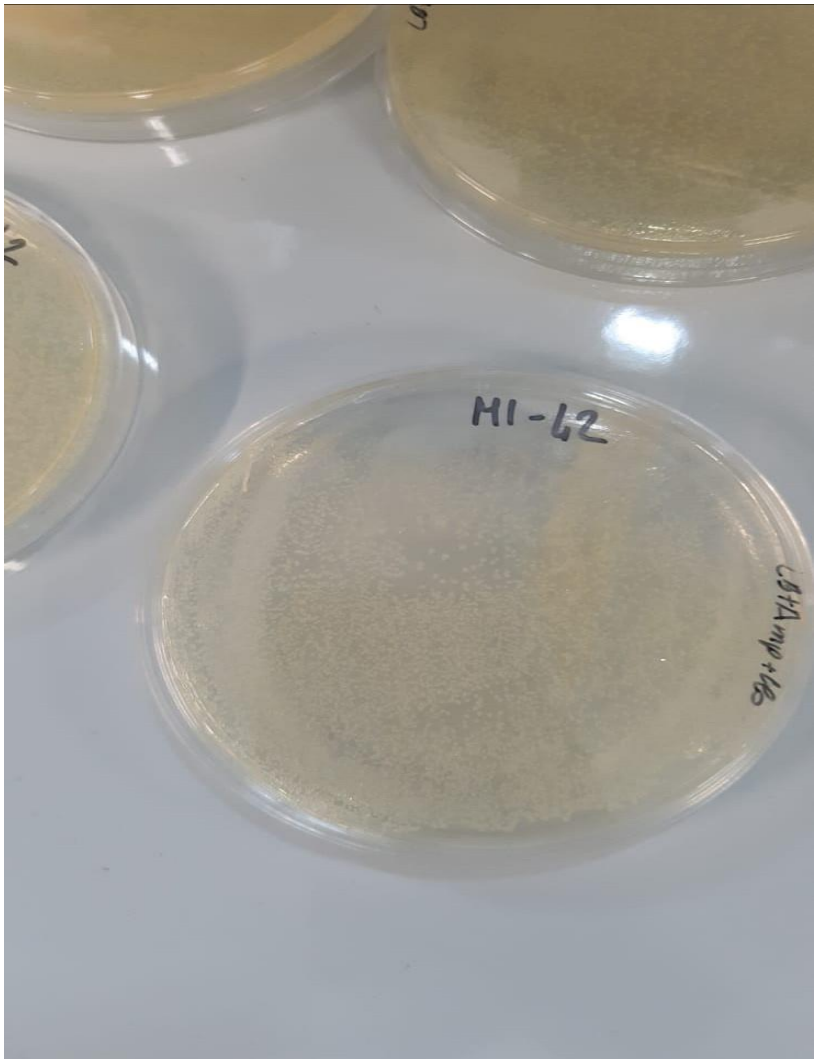

Figure 12: M1-42 Plate colture

The use of a small volume of transformed cells to be plated is chosen because this will avoid too massive growth that would make it difficult to collect single colonies in the next step. The following day, clones are inoculated in 10 mL of LB medium supplemented with ampicillin and chloramphenicol for pre-colture. The pre-culture was performed by adding 10 mL of LB, 10µL of Ampicillin, and Chloramphenicol. The cells were grown overnight in an orbital stirring at 37°C overnight. At this point is possible to freeze in glycerol.

Freezing in glycerol is carried out with 500 µL of 50% glycerol in which the chosen colony is diluted with a sterile tip. The whole is placed at -80 °C.

3.6.3 Protein expression

The bacterial culture of E.coli BL21, in 10 mL of LB with antibiotics is then inoculated in a 2L flask, containing 1L of LB with the antibiotics Ampicillin and Chloramphenicol at the concentrations mentioned above. This culture is incubated at 37°C at 220 rpm until it reaches a cell optical density of 0.4-0.45. (fig.13)

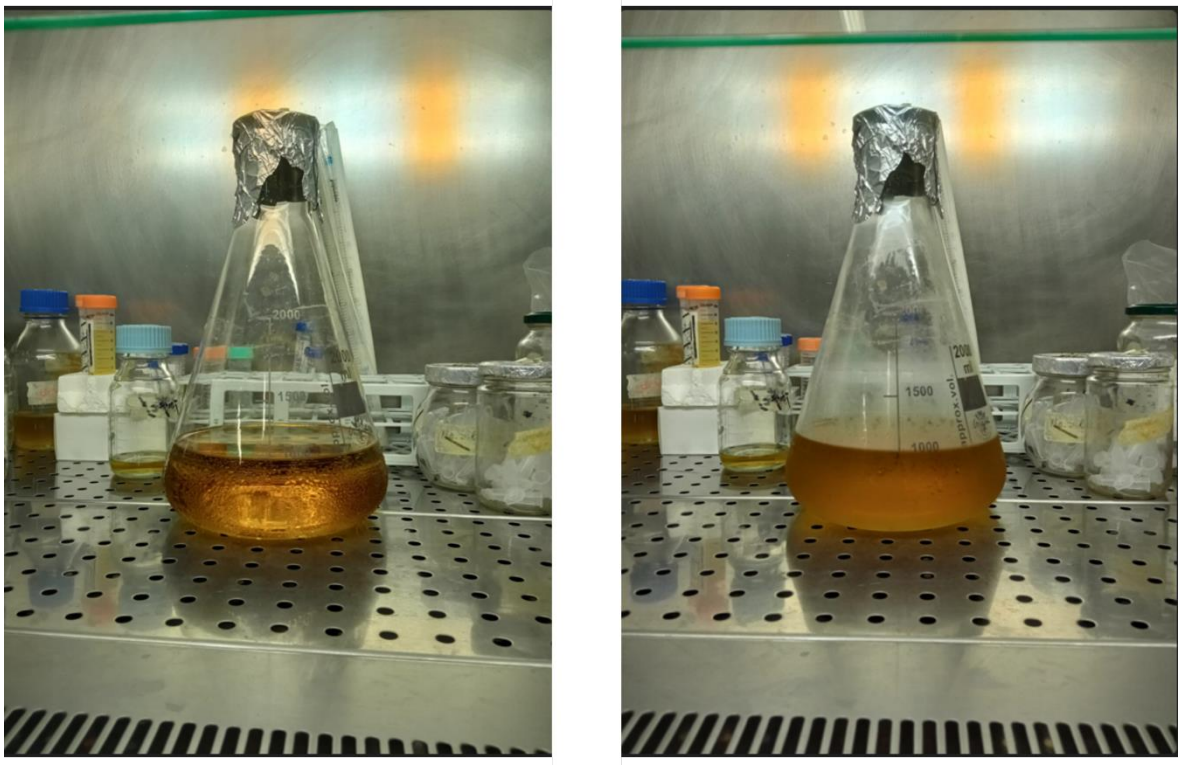

Figure 13: LB Colture before and after bacterial grown

Once the OD600 of the 1L Culture reaches 0.4-0.5, the expression of the protein is induced with the IPTG (Isopropyl-β-D-1-thiogalactopyranoside), until a final

concentration of 5 mM is reached in the 1 L of LB. The induction of IPTG must take place in the exponential growth phase to form insoluble inclusion bodies, which will be needed in the purification phase. The culture should be kept under agitation at 20°C overnight, in the presence of IPTG to allow the cells to express the Aβ peptide (M1-42). The next day the culture is centrifuged in falcon from 50 mL to 4000 x g for 15 min, the supernatant is removed and the pellet is kept at -80°C.

3.6.4. Cell lysis

The -80°C pellet is thawed on ice and resuspended in 30 mL of buffer A on ice. It was sonicated with a program that includes: 30s on, 30s off, for 5 cycles. The suspension was centrifuged at 4°C for 25 min at 4000 x g. The supernatant was removed and the remaining pellet was again resuspended in 30 mL of Buffer A and sonicated. The same procedure was repeated another time. After the last centrifugation, the supernatant is collected, and the pellet is stored. The washing steps are important to remove impurities from the inclusion bodies and to obtain a high final purity of the A beta. At this point, the pellet should be white and can be frozen until use or the solubilization process can be started for subsequent chromatography. All the supernatants obtained in the cell rupture process were analyzed by SDS-Page. The concentration of the

acrylamide gel used is 17% and the buffer used is TGS 1X. The marker used is VWR Protein Marker IV peqGOLD.

3.6.5 Protein purification

The pellet was placed on ice and after adding 15 mL of Buffer B it was sonicated for the last time and re-centrifuged. Subsequently, we proceed with dialysis, to eliminate the urea that cannot be in contact with the sample for more than 12 h because otherwise with its decomposition it forms isocyanic acid and carbamylate the terminal in N. The chromatographic system (ÄKTA FPLC) is held at 4°C. The column in which the gel-filtration of the protein was performed is Sephadex 10/300. The sample was loaded into the already equilibrated column and eluted with Buffer A. The absorbance was read at 280 nm to monitor the protein during the purification phase.

3.6.6. Analysis of the purified protein

3.6.6.1. SDS-Page and protein sequencing

The analysis of the protein took place over several moments. A first analysis was performed after the sonication of the protein on the various supernatants collected. By SDS-Page electrophoretic run, the band corresponding to the protein of interest was cut and sent for sequencing. A subsequent analysis again with the SDS page took place after the FPLC. Only the collected samples that were of interest were analyzed, as regards the elution of the protein.

3.6.6.2. Spectrophotometric determination of the protein concentration

The protein absorbance at 280 nm (A280nm) of 2 microliters of protein was determined with a spectrophotometer, appropriately calibrated in the protein storage buffer.

3.6.6.3. Small-angle X-Ray Scattering

Small-angle X-Ray Scattering (SAXS) measurements were performed at the BM29 beam-line of ESFR, the European Synchrotron (Grenoble, France) The investigated Aβ sample was at a concentration of 0.8 mg/mL, in the buffer A. SAXS curves were recorded at different temperatures. SAXS is a physical technique able to study size and shape of particles with nanometric dimensions randomly dispersed in solution. In the context of protein science, SAXS is considered one of the most suitable biophysical tool to study structure, interaction and aggregation of proteins in solution, including both folded and intrinsically disordered proteins (IDPs). SAXS can also provide useful information to decipher the thermodynamics and the kinetics of aggregation, including amyloid formation [51]. SAXS can analyze complexes of molecular size ranging from a few kDa to GDa and subject to various native or extreme experimental conditions (e.g. high pressure) [52] . The amount of structural information that can be obtained depends on the degree of supramolecular order of the sample. For example, in the case of diluted macromolecules in solution,

the shape, and the radius of gyration can be determined, while in the case of highly ordered fibers, a structural model for the molecular organization can be derived. In a SAXS experiment, it is necessary to use a collimated monochromatic X-ray beam that impinges the sample to be analyzed. The sample is typically placed in a quartz capillary.

When an X-ray beam hits a sample, the radiation can be partially scattered and partially absorbed. To avoid the detector damage a beamstop is positioned in the forward beam direction. The entire path that the radiation makes before and after the sample is kept under a high vacuum, to avoid scattering by air. The X-rays scattering is mainly due to electrons (Thomson scattering), and is mostly an elastic process. The incident and the scattering beams are described by the wave vector $\mathbf{k}_0$ and $\mathbf{k}_1$, which for an elastic process have the same modulus corresponding to $2\pi/\lambda$, λ being the X-ray wavelength.

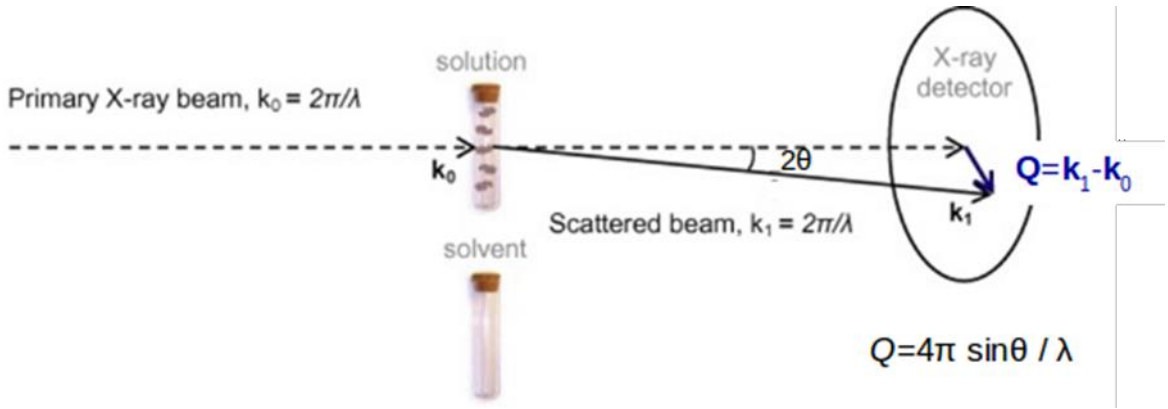

Figure 14: Schematic representation of a SAXS experiment

The scattered beam is recorded as a function of the momentum transfer (scattering vector) with modulus:

$$Q = \frac{4\pi \sin\theta}{\lambda} \quad (1)$$

where 2θ is the scattering angle equivalent to half the angle between incident radiation and scattered radiation. In a SAXS experiment with synchrotron light, the range of Q can extend over three orders of magnitude, for example at BM29 it ranges from 0.006 nm^{-1} to 6 nm^{-1}, corresponding in real space to dimensions ranging from 1µm to 1 nm. From a general point of view, the scattered beam intensity, more precisely defined as the macroscopical differential scattering cross section, corresponds to the square of the Fourier transform of electron density according to

$$I(\mathbf{Q}) = \frac{1}{V}\left\langle \left| \int_V d\mathbf{r}\, \rho(\mathbf{r}) e^{i\mathbf{Q}\cdot\mathbf{r}} \right|^2 \right\rangle \quad (2)$$

where V represents the volume of the irradiated sample, $\mathbf{r}$ is the position vector and $\rho(\mathbf{r})$ is the electron density. In addition, the angular brackets indicate that the squared Fourier transform is averaged over all possible configurations of the systems. For a meaningful analysis of the overall shape but also of the flexibility of a given protein, solutions containing single molecular species

without aggregates, i.e., monodisperse solutions, are generally required. Typically, a monodispersity greater than 95% is required for a successful structural analysis. In monodisperse solutions, in which all the particles in the solution are identical, have a constant electron density ρ_p different from the one of the solvent, ρ_0, and are randomly oriented, the scattering intensity is reduced to the following expression that only depends on the modulus Q:

$$I(Q) = n_p (\Delta\rho)^2 V_p^2 P(Q) S_M(Q) \quad (3)$$

where n_p is the number of particle per unit volume, $\Delta\rho = \rho_p - \rho_0$ is the contrast, V_p is the particle volume. The function $P(Q)$, called the form factor, represents the average of all the possible orientations of the vector $\mathbf{Q}$ (polar angles α_Q and β_Q) of the squared scattering amplitude:

$$P(Q) = \langle |F(\mathbf{Q})|^2 \rangle_{\alpha_Q, \beta_Q} \quad (4)$$

Where

$$F(\mathbf{Q}) = \frac{1}{V_p} \int_{V_p} d\mathbf{r}\, e^{i\mathbf{Q}\cdot\mathbf{r}} \quad (5)$$

Notice that the volume integral is calculated only within the volume of the particle. Hence, the form factor $P(Q)$ directly reflect the size as well as the shape of the particle. The function $S_M(Q)$ is defined as the "measured" structure factor and depends on the correlation between the positions of distinct particles.

If the system is diluted $S_M(Q) \approx 1$, hence the SAXS intensity is simply proportional to the particle form factor. On the other hand, for concentrated solutions, $S_M(Q)$, for small values of Q, can be either lower than 1, indicating particle repulsions or greater than 1, indicating the tendency of the particles to aggregate in the form, for example, of clusters.

Equation 3 clearly shows that the scattering intensity of the sample is proportional to the concentration: the higher the concentration, the better the signal-to-noise ratio of the data obtained from the interaction with the sample. On synchrotrons, the intense X-ray beam can cause radiation damage to the samples. To limit this damage, several means are used: beam attenuation and stabilizing additives in solution such as glycerol. On the other hand, for polydisperse systems, the SAXS intensity does not correspond to the form factor of a single particle, but rather to an average over the whole set of particles present in solution. However, even for polydisperse systems, general parameters can provide useful information on particle size and structural properties . According to the meaning of equation 3, the data obtained from the SAXS signal are typically represented by a so-called scattering curve, which reports the intensity $I(Q)$ as a function of Q. For diluted systems ($S_M(Q) \approx 1$), from the SAXS curve it is possible to determine various parameters, such as the radius of gyration (R_g) and the volume of particles in solution. In particular,

the radius of gyration, which gives information on the average size of the particle, is defined, for homogeneous particles, by the following expression:

$$R_g^2 = \frac{1}{V_p} \int_{V_p} r^2 d\mathbf{r} \tag{6}$$

In summary, SAXS curves contain information about shape, size, and distance between the particles. This information can be distinguished by several methods. A first group of methods are focused on the derivation of the particle shape and hence they are referred to as shape-reconstruction methods. They make use of advanced mathematical tools, such as the expansion in series of spherical harmonics of $F(\mathbf{Q})$ [53] Other methods assume a simple model for the particle geometry (spheres, cylinders, ellipsoids, etc.) try to optimize the geometrical parameter by the optimum fit of SAXS experimental data.

GUINIER ANALYSIS

The radius of gyration can be obtained through Guinier's law, which is valid for diluted systems at low values of Q,

$$I(Q) \approx I(0) e^{-Q^2 R_g^2/3} \tag{7}$$

It introduces a good approximation of $I(Q)$ as long as the condition $Q_{\max} R_g < 1.3$ exists, where $Q_{\max}$ is the maximum value of Q on which to analyze the data. By considering the logarithm of equation 6, we obtain

$$\log I(Q) \approx \log I(0) - \frac{1}{3} Q^2 R_g^2 \quad (8)$$

Hence by reporting data in the form of the so-called Guiner plot, $\log I(Q)$ vs. Q^2, at low Q a straight line is detected and, from its slope, the radius of gyration can be easily calculated.

GUINIER ROD-LIKE ANALYSIS

If the particles are in the form of rigid rods (such as amyloid fibrils), with length much larger than their radius, the so-called cross-section radius R_c can be calculated by applying the Guinier rod-like law,

$$QI(Q) \approx QI(0) e^{-Q^2 R_c^2/2} \quad (9)$$

Indeed, by considering the logarithm of equation 8, we obtain

$$\log[QI(Q)] \approx \log[QI(0)] - \frac{1}{2} Q^2 R_c^2 \quad (10)$$

Hence by reporting data in the form of $\log[QI(Q)]$ vs. Q^2, at low Q a straight line is detected and, from its slope, the radius of the cross section can be easily calculated.

KRATKY ANALYSIS

Kratky's analysis is a simple method that consists of representing SAXS data in a plot of $Q^2I(Q)$ vs. Q.

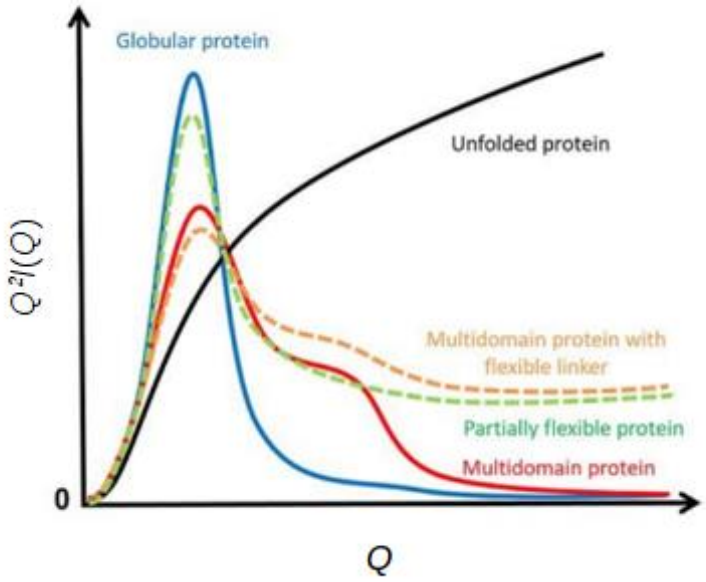

Figure 15: Krakty plot

From the Kratky plot, it is possible to obtain information about the state of a protein that can have a compact, unfolded, or partially unfolded structure, characteristic of the intermediate states of folding. (Fig.10)

In the Kratky plot, disordered proteins have a high Q plateau, while compact globular proteins will have a bell-shaped peak. A partially disordered protein (unfolded chain) may have a combination of the bell shape and the plateau, or a plateau that slowly decays to zero.

3.6.6.4. Functional assays with Thioflavin T in fluorescence spectrometry

In fluorescence spectroscopy a light source, usually ultraviolet, excites the electrons which, by decaying, emit light (fluorescence), usually in the visible range, but not necessarily. Mainly the electrons of the electronic and vibrational states are involved. Each molecule has various states, called energy levels. The fundamental electronic level is found at lower energy, while the excited electronic levels are found at higher energies. Within each electronic level, there are various vibrational levels. In fluorescence spectroscopy, through the absorption of a photon, the molecule passes from the lowest energy vibrational level of the fundamental electronic level (which is the most populated at room temperature, according to Boltzmann's statistical distribution) to one of the vibrational levels of the first electronic excited state. Once excited, the

photoluminescent molecule can lose the excess energy absorbed through various relaxation mechanisms, which can be viewed in the Jablonski diagram. Immediately after the absorption of the photon, the molecule loses the excess vibrational energy (for example through collision with the other molecules in the sample), decaying at the lowest vibrational level of the excited electronic state (vibrational relaxation). Subsequently, the molecule decays into one of the vibrational levels of the fundamental electronic level, emitting a photon in the decay process, which can have different energies or frequencies. With fluorescence spectroscopy, it is possible to determine the structure of the different vibrational levels by analyzing the different frequencies of the light emitted, with their relative intensities. Fluorescence spectra are of two types: emission spectra and excitation spectra. The emission spectrum of a

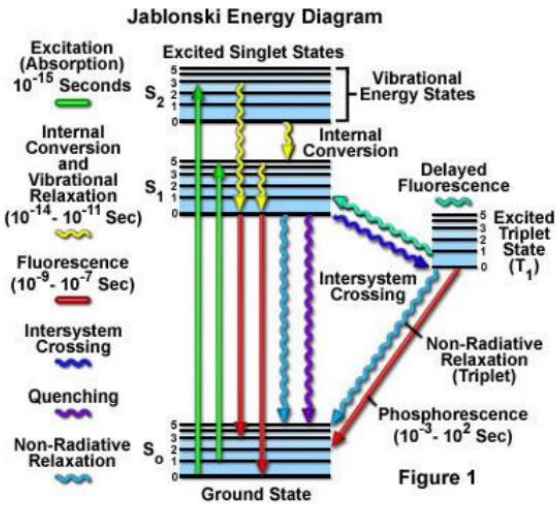

Figure 16:Jablonski diagram.

photoluminescent molecule is obtained by keeping the excitation wavelength

fixed (usually a wavelength with high absorbance is chosen) and measuring, with a monochromator, the intensity of fluorescence emitted by the molecule at selected wavelengths. The excitation spectrum of a photoluminescent molecule is obtained by varying the excitation wavelength and measuring, with a monochromator, the fluorescence emission at a constant wavelength. Part of the incident light is absorbed by the sample and part of the sample molecules fluoresces. Fluorescent light is emitted in all directions. Part of the light emitted passes through a second filter or monochromator and reaches the detector, usually placed at 90 ° to the incident beam, to minimize the risk that the incident light transmitted or reflected reaches the detector. Fluorimeters with two monochromators and one continuous light source can record both emission spectra and excitation spectra. The experiment in ThT with the Abeta samples were performed changing the Abeta and ThT concentration. [54]

Chapter Four

RESULTS

4.1 Production and purification of Aβ

Production trials of both plasmids were made to produce Aβ40 and Aβ42. Various conditions were tested before obtaining optimal productions. To note, the protocol that made it possible to obtain Aβ42 is not useful to obtain Aβ40. First of all, an electrophoretic run-in agarose gel was performed after the plasmid extraction to evaluate its actual presence. (fig.16)

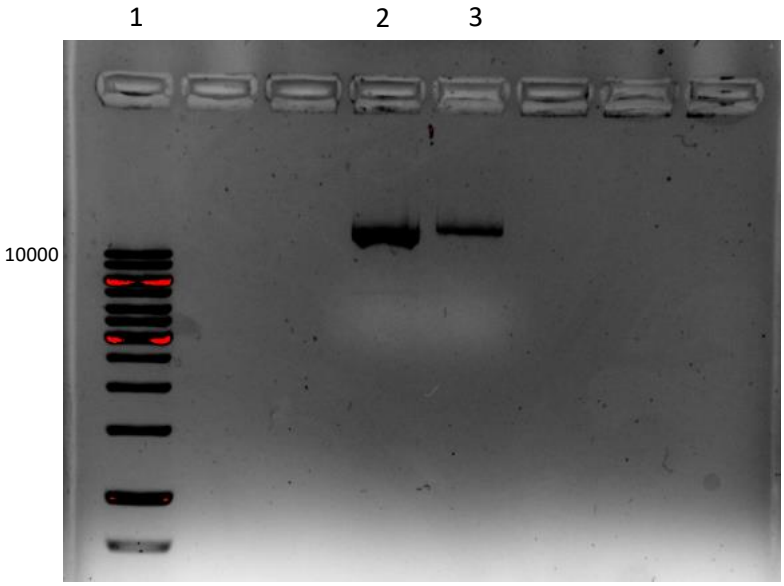

Figure 16: Agarose gel, (1) marker,(2) plasmid Abeta40, (3)plasmid Abeta42

4.2 Aβ analysis

4.2.1 SDS-Page

The first SDS page was performed after the sonication and breaking of the pellets. As it can be seen in Figure 16, the two proteins have different responses to the protocol: Aβ40 is not expressed, while Aβ42 is clearly visible (Fig.17).

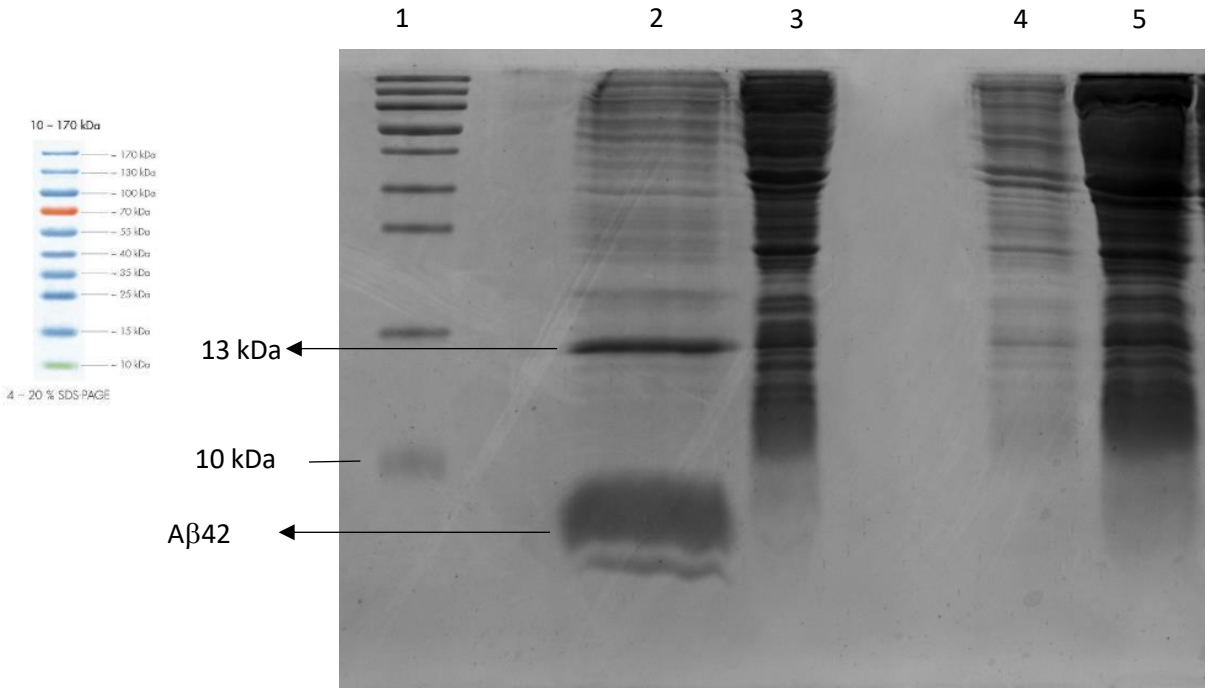

Figure 17: SDSpage of the sonicate; (1) marker, (2) final pellet solubilized with urea from Aβ42, (3) Supernatant 2 from Aβ42, (4) pellet solubilized with urea from Aβ40, (5) Supernatant 2 from Aβ40.

Our attention was then focused only on the Aβ42.

One of the main problems encountered in the purification of the protein was the method of elimination of urea, necessary to solubilize the inclusion bodies. Two different approaches were evaluated: ultracentrifugation and dialysis (Fig.18).

Figure 18: dialysis vs. ultracentrifugaiton

Dialysis (3.5 kDa cut-off) is the simplest method and by using the right dialysis filters, urea can be diluted after several steps until it is dissolved.

The ultracentrifugation method (cut off 10.0 kDa) through a concentrator is faster, but the protein, being very affected by centrifugation and continuous manipulation, tends to aggregate and the quantity that remains adhered to the walls of the filter is considerable (Fig.19).

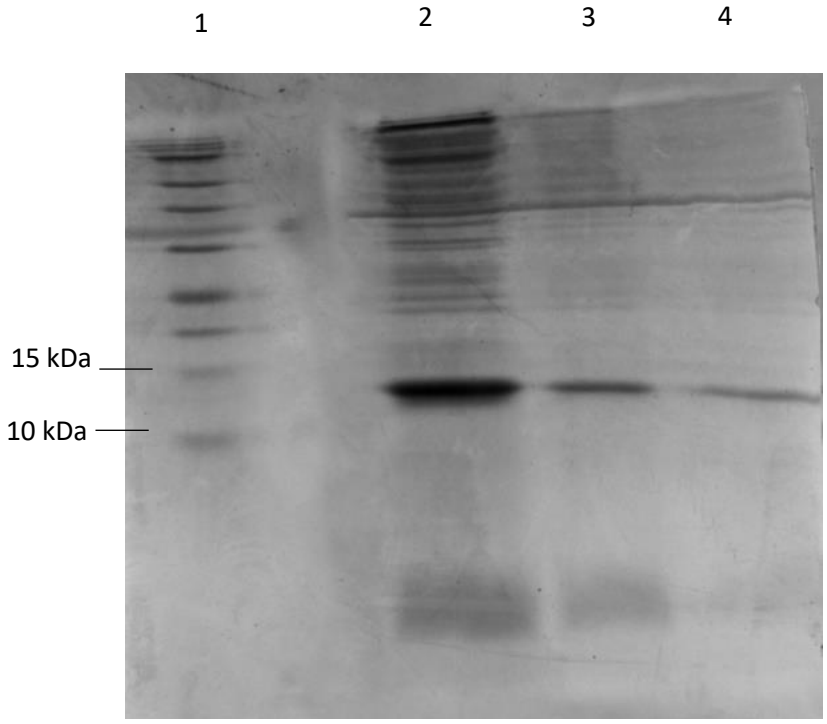

Figure 19: (1) marker, (2) solution before ultracentrifugation, (2) dialysate solution (3) solution after ultracentrifugation

A new SDS page was then performed after the FPLC. Only the useful fractions were run where the protein was expressed (Fig.20).

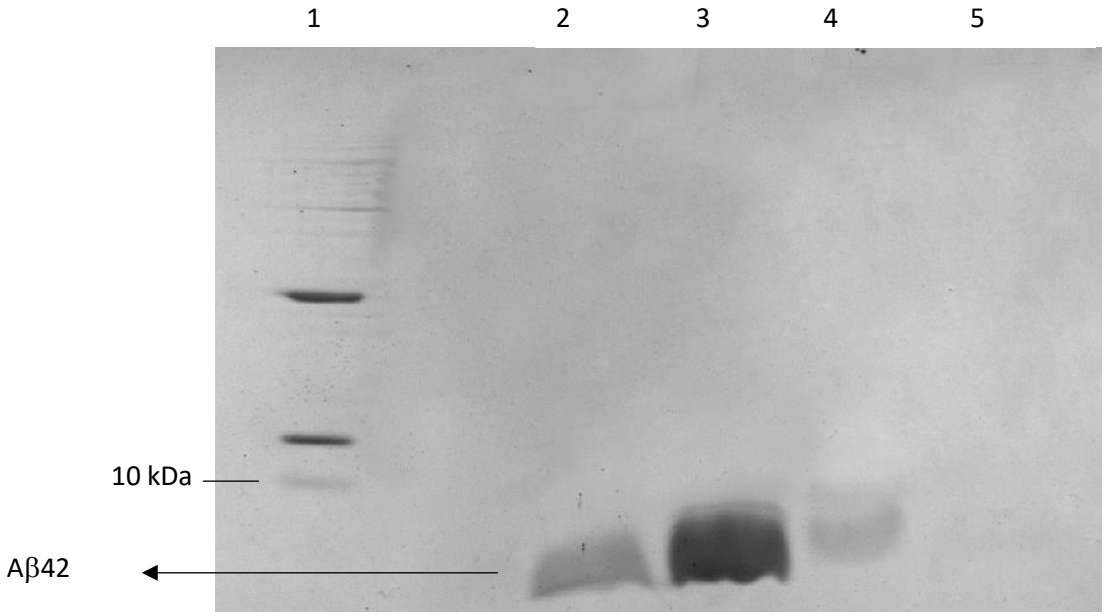

Figure 20 : (1) marker, (2) fraction 26, (3) fraction 27, (4) fraction 28, (5)fraction 29

The final concentration of the resulting protein with the maximum dialysis obtained was 1 mg/mL.

4.2.2 Sequencing

Sequencing was performed by cutting from this gel:

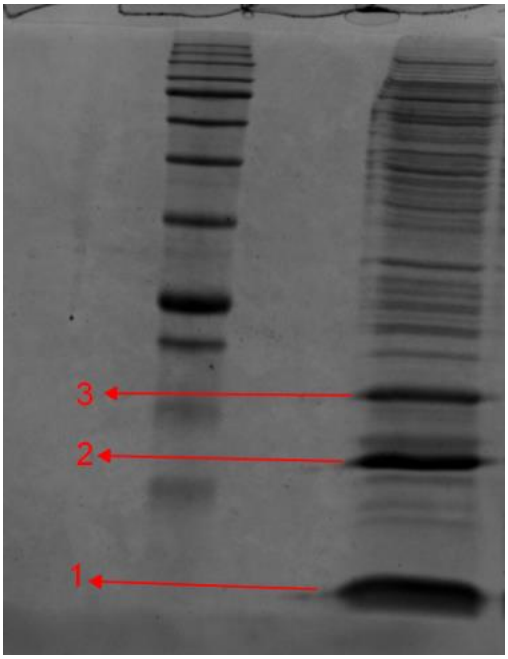

Figure 21: SDS Abeta42

4.2.3 Small-angle X-Ray Scattering

Small-angle x-ray scattering measurements were performed at the BM29 beamline of ESRF, the European synchrotron Grenoble (France). The analyzed samples consist of Aβ at a concentration of 0.8 mg/mL. SAXS curves were recorded at 20, 30, 40 and 50 °C. The data reduction process, that basically includes the empty capillary and the buffer subtraction and the absolute calibration, has been carefully carried out by means of a home-made software, since results obtained with the available software at the BM29 beamline were not satisfactory.

SAXS curves, originated by the data reduction process, are shown in a standard semi-logarithmic plot in Figure 22. Curves are slightly depending on the temperature and show an up-turn at low *q,* a signature of the presence of aggregated species.

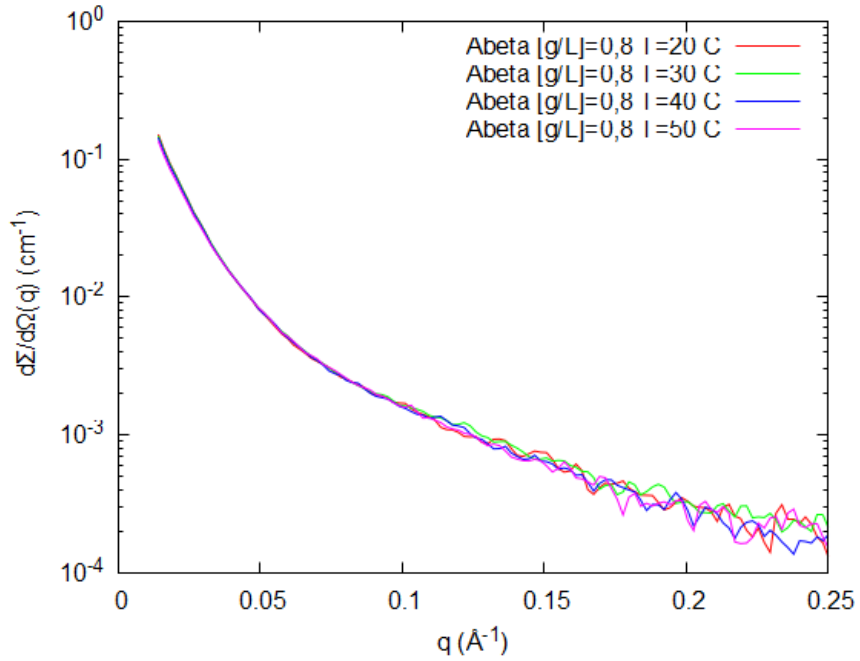

Figure 22. SAXS curves of Ab samples.

Corresponding Kratky plots, obtained using Gnuplot software, are reported in Figure 23.

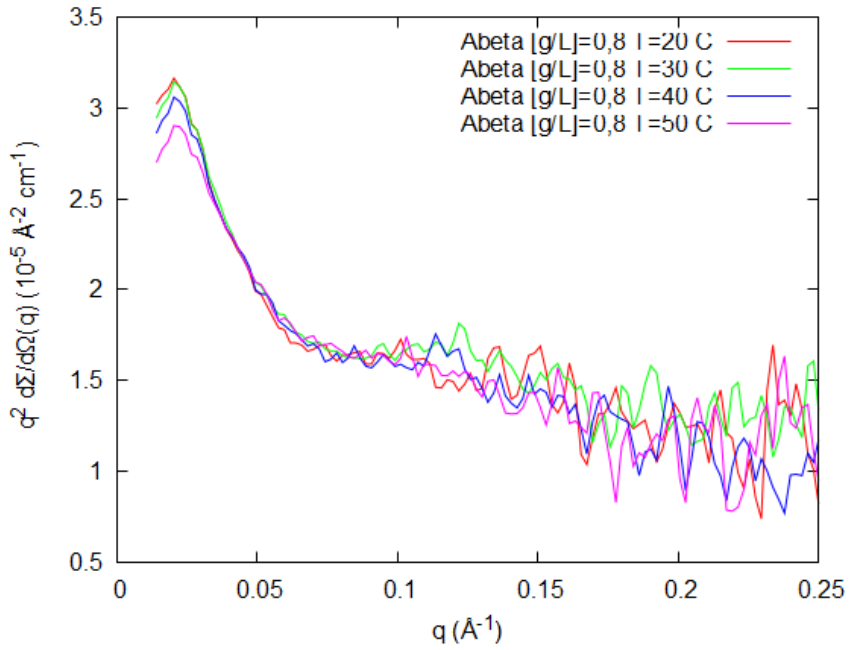

Figure 23. Kratky plots of Ab SAXS curves.

Here it can be better appreciated that, as the temperature increases, the intensity of the curve slightly decreases, without a marked modification of the curve feature. The phenomenon can simply be attributed to the variation of the water density with temperature. Most importantly, the absence of a flat plateau at high q indicates that proteins, at any temperature, are in compact states and no signature of unfolded monomers is perceived. This information, combined with the observation of the semi-logarithmic curves of Figure 22, confirm the presence of large and compact protein states. In order to verify if such compact states are in a fibrillar form, the set of data has been subsequently reported in the form of Guinier rod-like plot, shown in Figure 24.

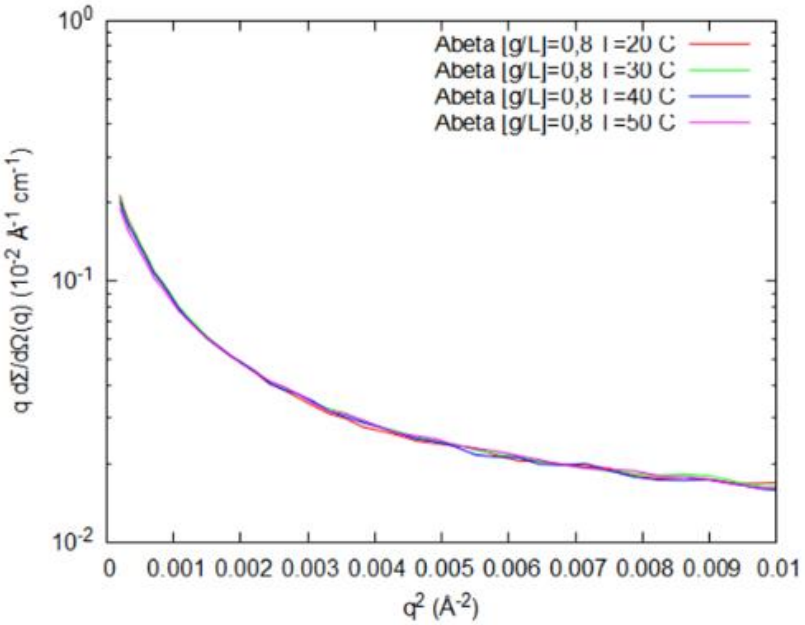

Figure 24. Guinier rod-like plots of SAXS data.

It is not possible to observe a *q* range in which curves, reported in this type of plot, assume an almost linear behaviour, which would have been a clear indication of the presence of rod-like particles, such as amyloid fibrils.

In summary, the overall picture that emerges from SAXS experiments is the one of Aβ proteins that form compact, aggregate and non-fibrillar structures. Probably such structures are oligomers that have been formed during when the protein has been resuspended in the buffer. Further interpretation of the data is far from being easy, and more data are necessary to better describe the structure of the examined protein.

4.3 Thioflavin T assay

After purification, thioflavin aggregation assays were performed. The assays were performed in PBS. Different concentrations of Thioflavin T (taken from stock 500 μM) 5, 10, 25 μM, and different concentrations of Aβ, 5, 15, and 25 μM were tested. The Aβ was in buffer A. The final volume tested was 200 μL. The maximum analysis time was 48 h. The samples were placed at 37 ° C in motion. 10 times were taken, as shown in the table:

t1	t2	t3	t4	t5	t6	t7	t8	t9	t10
0.5 h	1 h	1.5 h	2 h	2.5h	3 h	3.5	4 h	24 h	48 h

The first screening protocol of the Thioflavin T assay yielded the following results:

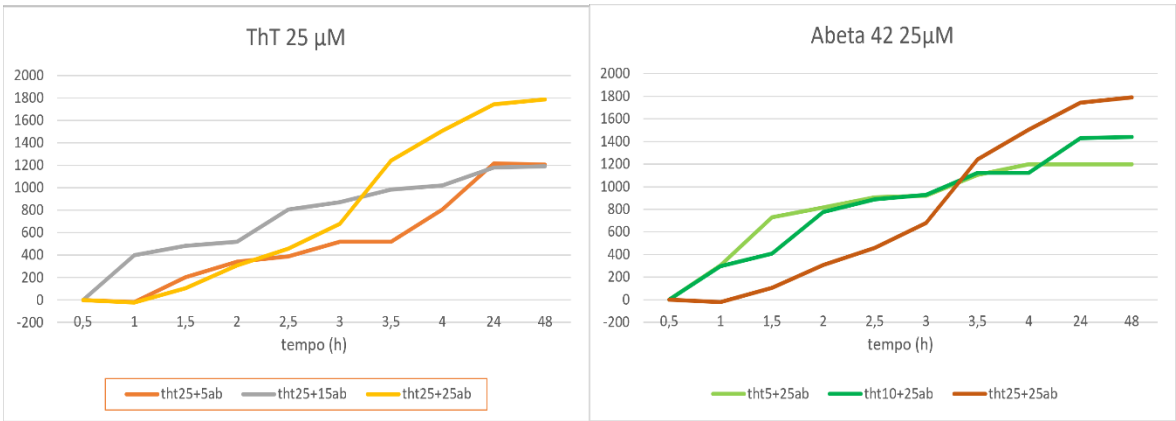

Figura 15: First graphs costant Tioflavin T with different Abeta concentrations: 5 µM, 15 µM, 25 µM. Second graphs constant Abeta 42 concentration and differents ThT: 5 µM,10 µM, 25 µM.

Comparing the two graphs, we note how the trend is increasing and how the ratio of ThT and Aβ 1:1 produces a better fluorescence. As the concentration of thioflavin increases, there is an increase in the final reading of the Aβ. In the case of the maximum concentration analyzed, we see how the final value rises even after the other two experiments. Generally, the formation of fibrils should take place in an average time of about two hours under controlled conditions (T and agitation). In the graphs below, we can see with the ratio of 1:1 is no longer visibly advantageous. The reading seems to depend on the concentration of Thioflavin. (fig.26; fig.27).

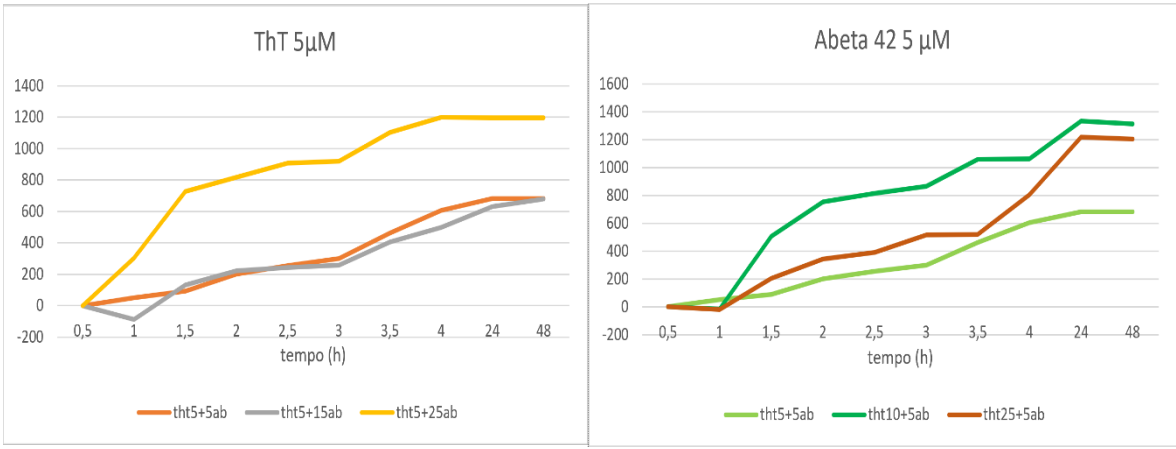

Figure 26: First graphs costant Tioflavin T with different Abeta concentrations: 5 µM, 15 µM, 25 µM. Second graphs constant Abeta 42 concentration and differents ThT: 5 µM,10 µM, 25 µM.

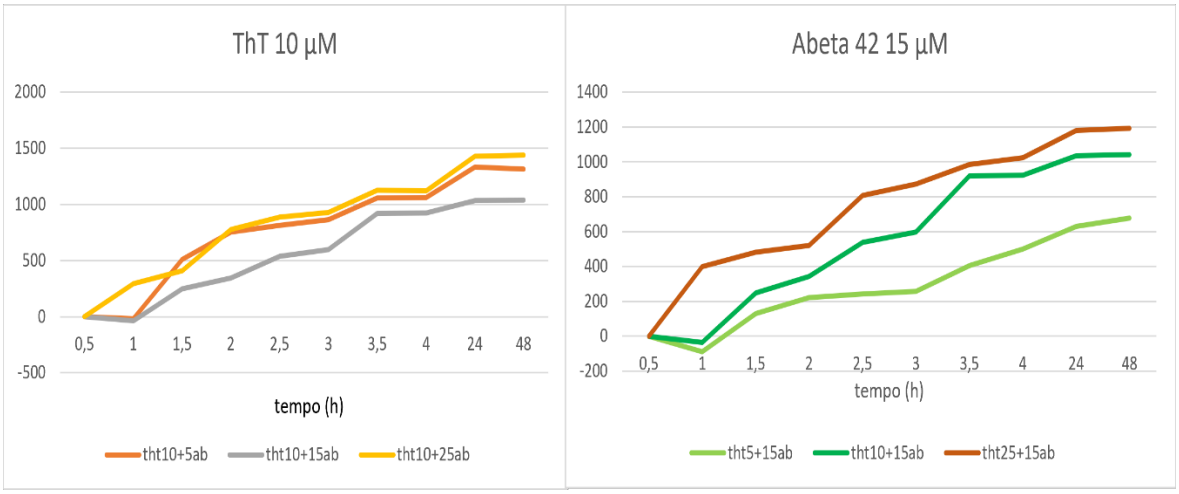

Figure 27: First graphs costant Tioflavin T with different Abeta concentrations: 5 µM, 15 µM, 25 µM. Second graphs constant Abeta 42 concentration and differents ThT: 5 µM,10 µM, 25 µM.

In the graph below, we have a summary of all the reads in ThT. The general trend shows that as expected, the fluorescence arises in time, which is one of the signs that we are in presence of amyloid aggregates. (fig.28)

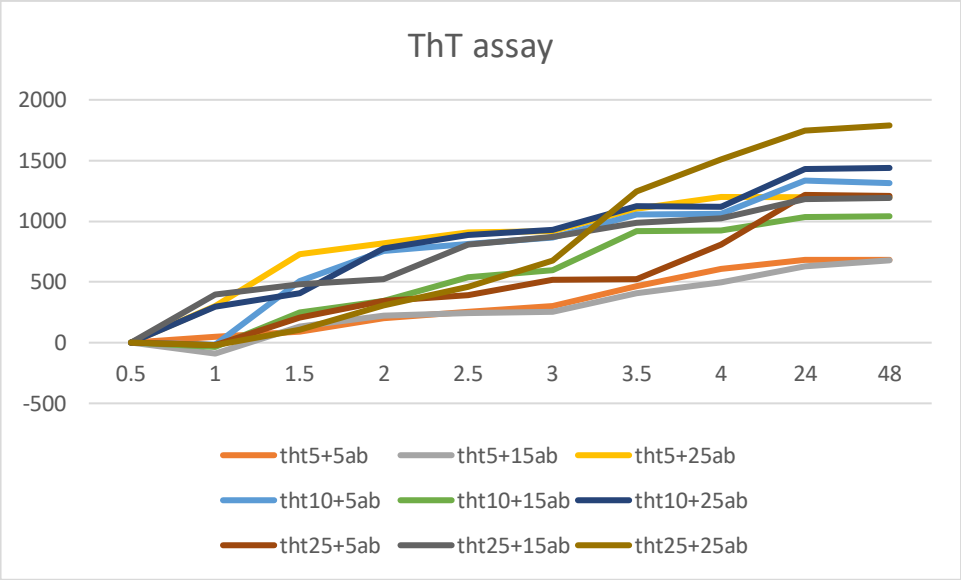

Figure 28: Summary with all the reads.

Chapter Five

CONCLUSIONS

My thesis focused on the production of the beta amyloid protein, in a simple and relatively fast way. Various factors contributed to the production of this protein, the fact that the promoter of the plasmid was a very strong promoter (T7), made it possible, under induction, a production of the protein in large quantity in the inclusion bodies of Coli BL21. The production in the inclusion bodies, in this case, was a helping factor, as the protein remains isolated from all other cellular components and can be purified by simply breaking the inclusion bodies. One of the key factors in the study of beta amyloid protein (especially 42) is having it in monomeric form, that with this protocol it is obtained, even if for a limited time. Thanks to its production, it was possible to perform preliminary SAXS studies of the early aggregated protein structures. Moreover, following sequencing data and thioflavin assays, it was possible, both to assess the correctness of the produced protein and to measure its response to the fluorescent dye, according to literature results. In particular, the optimal concentration of 25 μM of ThT and Aβ reflects the 1:1 recommended ratio in this assay.

Thanks to the possibility of obtaining a recombinant Aβ, it will be possible in the future to deeply study its structure and the multiple conformational states that it forms related to the physical-chemical conditions. In such way, by using different experimental approaches starting with the use of the recombinant

protein obtained by our method, in combination with computer simulations based on atomistic or coarse-grain Molecular Dynamics, it will be possible to understand how Aβ assemblies, fibrils, and, most importantly, which strategies can be applied to investigate its inhibition.

BIBLIOGRAPHY

[1] Werner Kaminksy, Lee-Way Jin, Steven Powell, Izumi Maezawa, Kacey Claborn, Charles Branham, Bart Kahr,Polarimetric imaging of amyloid, Micron,Volume 37, Issue 4,2006, Pages 324-338,

[2] Margaret Sunde, Colin Blake,The Structure of Amyloid Fibrils by Electron Microscopy and X-Ray Diffraction, Editor(s): Frederic M. Richards, David S. Eisenberg, Peter S. Kim, Advances in Protein Chemistry, Academic Press,Volume 50.

[3;12;13] Kirkitadze MD, Kowalska A. Molecular mechanisms initiating amyloid beta-fibril formation in Alzheimer's disease. Acta Biochim Pol. 2005;52(2):417-23. Epub 2005 May 31. PMID: 15933761.

[4;5;10;22,24,28] Mattson MP. Pathways towards and away from Alzheimer's disease. Nature. 2004 Aug 5;430(7000):631-9. doi: 10.1038/nature02621. PMID: 15295589; PMCID: PMC3091392.

[6] APP - Amyloid-beta precursor protein precursor - Homo sapiens (Human) - APP gene & protein. (s.d.). UniProt. https://www.uniprot.org/uniprot/P05067

[7;11] Zheng H, Koo EH. The amyloid precursor protein: beyond amyloid. Mol Neurodegener. 2006 Jul 3;1:5. doi: 10.1186/1750-1326-1-5. PMID: 16930452; PMCID: PMC1538601.

[8] Wenstrup, R. J., Smith, S. M., Florer, J. B., Zhang, G., Beason, D. P., Seegmiller, R. E., Soslowsky, L. J., & Birk, D. E. (2011). Regulation of

collagen fibril nucleation and initial fibril assembly involves coordinate interactions with collagens V and XI in developing tendon. The Journal of biological chemistry, 286(23), 20455–20465. https://doi.org/10.1074/jbc.M111.223693

[9] Zhang, Yw., Thompson, R., Zhang, H. et al. APP processing in Alzheimer's disease. Mol Brain 4, 3 (2011). https://doi.org/10.1186/1756-6606-4-3

[14] Wildsmith, K.R., Holley, M., Savage, J.C. et al. Evidence for impaired amyloid β clearance in Alzheimer's disease. Alz Res Therapy 5, 33 (2013). https://doi.org/10.1186/alzrt187

[15] Hardy J. Amyloid, the presenilins and Alzheimer's disease. Trends Neurosci. 1997 Apr;20(4):154-9. doi: 10.1016/s0166-2236(96)01030-2. PMID: 9106355.

[16] Woojin Kim, Michael H. Hecht,Sequence Determinants of Enhanced Amyloidogenicity of Alzheimer Aβ42 Peptide Relative to Aβ40*,Journal of Biological Chemistry,Volume 280, Issue 41,2005,Pages 35069-35076, ISSN 00219258,https://doi.org/10.1074/jbc.M505763200.(https://www.sciencedirect.com/science/article/pii/S0021925820639473)

[17,19] Meinhardt J, Tartaglia GG, Pawar A, et al. Similarities in the thermodynamics and kinetics of aggregation of disease-related Abeta(1-40) peptides. Protein Sci. 2007;16(6):1214-1222. doi:10.1110/ps.062734207

[18] Meinhardt J, Tartaglia GG, Pawar A, et al. Similarities in the thermodynamics and kinetics of aggregation of disease-related Abeta(1-40) peptides. Protein Sci. 2007;16(6):1214-1222. doi:10.1110/ps.062734207

[20] Bitan G, Kirkitadze MD, Lomakin A, Vollers SS, Benedek GB, Teplow DB. Amyloid beta -protein (Abeta) assembly: Abeta 40 and Abeta 42 oligomerize through distinct pathways. Proc Natl Acad Sci U S A. 2003;100(1):330-335. doi:10.1073/pnas.222681699

[21] Sergiu Huleani, Michael R. Roberts, Lucy Beales, Emmanouil H. Papaioannou. (2022) Escherichia coli as an antibody expression host for the production of diagnostic proteins: significance and expression. Critical Reviews in Biotechnology 42:5, pages 756-773.

[22] Haughey NJ, Nath A, Chan SL, Borchard AC, Rao MS, Mattson MP. Disruption of neurogenesis by amyloid beta-peptide, and perturbed neural progenitor cell homeostasis, in models of Alzheimer's disease. J Neurochem. 2002 Dec;83(6):1509-24. doi: 10.1046/j.1471-4159.2002.01267.x. PMID: 12472904.

[24] Kenjiro Ono,Alzheimer's disease as oligomeropathy,Neurochemistry International,Volume 119,2018,Pages 57-70,ISSN 0197-0186,https://doi.org/10.1016/j.neuint.2017.08.010.

[26] Mattson MP, Chan SL, Duan W. 2002. Modification of brain aging and neurodegenerative disorders by genes, diet, and behavior. Physiol Rev. 82:637-672.

[27] Saido T, Leissring MA. Proteolytic degradation of amyloid β-protein. Cold Spring Harb Perspect Med. 2012;2(6):a006379. doi:10.1101/cshperspect.a006379

[28] D. Gabuzda, J. Busciglio, L.B. Chen, P. Matsudaira, B.A. Yankner, Inhibition of energy metabolism alters the processing of amyloid precursor protein and induces a potentially amyloidogenic derivative., Journal of Biological Chemistry,Volume 269, Issue 18,1994,Pages 13623-13628,ISSN 0021-9258,https://doi.org/10.1016/S0021-9258(17)36875-8.

[30] Baglioni S, Casamenti F, Bucciantini M, et al. Prefibrillar amyloid aggregates could be generic toxins in higher organisms. J Neurosci. 2006;26(31):8160-8167. doi:10.1523/JNEUROSCI.4809-05.2006

[31] Louise C Serpell,Alzheimer's amyloid fibrils: structure and assembly,Biochimica et Biophysica Acta (BBA) - Molecular Basis of Disease,Volume 1502, Issue 1,2000,Pages 16-30,ISSN 0925-4439,https://doi.org/10.1016/S0925-4439(00)00029-6.

[31] Bucciantini M, Giannoni E, Chiti F, Baroni F, Formigli L, Zurdo J, Taddei N, Ramponi G, Dobson CM, Stefani M (2002). Inherent toxicity of aggregates

implies a common mechanism for protein misfolding diseases. Nature 416:507–511

[32,33,43] Stefani M. (2004), Protein misfolding and aggregation: new examples in medicine and biology of the dark side of the protein world, Biochimica et Biophisica Acta, 1739: 5- 25.

[34] Gazit E. (2005), Mechanisms of amyloid fibril self-assembly and inhibition. Model short peptides as a key research tool, The FEBS journal, 272(23): 5971-8.

[35] Nilsson M.R. (2004), Techniques to study amyloid fibril formation in vitro, Methods, 34: 151-160.

[36;37] LeVine H. (1997), Stopped-flow kinetics reveal multiple phases of Thioflavin T binding to Alzheimer β(1-40) amyloid fibrils, Archives of Biochemistry and Biophysic, 342: 306-316.

[38] Voropai E.S., Samtsov M.P., Kaplevskii K.N., Maskevich A.A., Stepuro V.I., Povarova O.I., Kuznetsova I.M., Turoverov K.K., Fink A.L., Uverskii V.N. (2003), Spectral properties of thioflavin T and its complexes with amyloid fibrils, Journal of Applied Spectroscopy, 70: 868-874.

[40] Jarrett J.T., Berger E.P., Lansbury P.T. Jr. (1993), The carboxy terminus of the beta amyloid protein is critical for the seeding of amyloid formation:

implications for the pathogenesis of Alzheimer's disease, Biochemistry, 32: 4693-4697.

[41] Lomakin A., Chung D.S., Benedek G.B., Kirschner D.A., Teplow D.B.(1996), On the nucleation and growth of amyloid beta-protein fibrils: detection of nuclei and quantitation of rate constants, Proceedings of the National Academy of Sciences USA, 93(3): 1125-9.

[42] Iannuzzi C, Irace G, Sirangelo I. The Effect of Glycosaminoglycans (GAGs) on Amyloid Aggregation and Toxicity. Molecules. 2015; 20(2):2510-2528. https://doi.org/10.3390/molecules20022510

[43] Murphy R.M. (2002), Peptide aggregation in neurodegenerative disease, Annual review of biomedical engineering, 4: 155-74.

[44;46;47] Walsh D.M., Hartley D.M., Kusumoto Y., Fezoui Y., Condron M.M., Lomakin A., Benedek G.B., Selkoe D.J., Teplow D.B. (1999), Amyloid β-protein fibrillogenesis (structure and biological activity of protofibrillar intermediates), Journal of Biological Chemistry, 274: 25945-25952.

[45] Goldsbury C.S., Wirtz S.,. Muller S.A., Sunderji S., Wicki P., Aebi U., Frey P. (2000), Studies on the in vitro assembly of Abeta 1-40: implications for the search for A beta fibril formation inhibitors, Journal of Structural Biology, 130: 217-231.

[48] Zerovnik E.(2002), Amyloid-fibril formation. Proposed mechanisms and relevance to conformational disease, European Journal of Biochemistry, 269(14): 3362-71.

[49] ACS Chem. Neurosci. 2020, 11, 20, 3204–3213 Publication Date:September 22 2020https://doi.org/10.1021/acschemneuro.0c00300

[50] Walsh DM, Thulin E, Minogue AM, Gustavsson N, Pang E, Teplow DB, Linse S. A facile method for expression and purification of the Alzheimer's disease-associated amyloid beta-peptide. FEBS J. 2009 Mar;276(5):1266-81. doi: 10.1111/j.1742-4658.2008.06862.x. PMID: 19175671; PMCID: PMC2702495.

[51C. Ricci, F. Spinozzi, P. Mariani, and M. G. Ortore. Protein Amyloidogenesis Investigated by Small-angle Scattering. Current Pharmaceutical Design, 22:3937–3949, 2016

[52] D. Russo, M. G. Ortore, F. Spinozzi, P. Mariani, C. Loupiac, B. Annighofer, and A. Paciaroni. The impact of high hydrostatic pressure on structure and dynamics of β-lactoglobulin. Biochim. Biophys. Acta, 183:4974–4980, 2013.

[53] F. Spinozzi, F. Carsughi, and P. Mariani. Particle shape reconstruction by Small-Angle Scattering. Integration of group theory and maximum entropy to multipole expansion method. J. Chem. Phys., 109:10148–10158, 1998.

[54] Xue, C., Lin, T. Y., Chang, D., & Guo, Z. (2017). Thioflavin T as an amyloid dye: fibril quantification, optimal concentration and effect on aggregation. *Royal Society open science*, *4*(1), 160696. https://doi.org/10.1098/rsos.160696.